A citrullination-ubiquitination pathway controls pre-meiotic H1 eviction and is essential for gametogenesis in *Arabidopsis*

Yanru Li[1,4], Danli Fei[1,4], Jasmin Schubert[1,4], Kinga Rutowicz[1,2], Zuzanna Kaczmarska[3], Alberto Linares[1], Alejandro Giraldo Fonseca[1], Sylvain Bischof[1], Ueli Grossniklaus[1] and Célia Baroux[1,5,*]

AFFILIATIONS

1. Department of Plant and Microbial Biology & Zurich-Basel Plant Science Center, University of Zurich, Zurich, Switzerland
2. Laboratory of Protein Structure, International Institute of Molecular and Cell Biology, Warsaw, Poland
3. Present address: Institute of Molecular Plant Biology, ETH Zurich, Zurich, Switzerland
4. Contributed equally
5. Lead contact

* Correspondence: cbaroux@botinst.uzh.ch

KEYWORDS

Linker histone, citrullination, ubiquitination, meiosis, gametogenesis, *Arabidopsis*

SUMMARY

In flowering plants, the transition from somatic to reproductive cell fate is marked by the differentiation of spore mother cells (SMCs), the functional equivalent of animal primordial germ cells (PGCs). Like their animal counterparts, SMCs undergo extensive structural and compositional changes in chromatin, initiated by the loss of linker histones, in a stepwise process. To investigate the role and mechanism of H1 eviction, we focused on two candidate pathways. Our findings show that specific point mutations, affecting either a putative citrullination site or ubiquitination site, prevent the eviction of H1.1 in the SMCs. Additionally, downregulation or chemical inhibition of the AIH citrulinase (Agmatine Imino Hydrolase) or of the E3-Ubiqtuitin ligase CULLIN4 also results in the persistence of H1.1 in SMCs. Notably, SMCs with impaired H1.1 eviction exhibit mild defects in chromatin reorganization and cell elongation. Despite these defects, the SMCs proceed through meiosis but fail to complete gametogenesis. Collectively, we propose a citrullination-ubiquitination pathway governing pre-meiotic H1 eviction as a critical mechanism for establishing post-meiotic competence in the *Arabidopsis* germline.

INTRODUCTION

Sexually reproducing multicellular organisms generate a specialized cell lineage dedicated to meiosis and gametogenesis, two processes that are fundamental to ensuring genetic diversity while maintaining chromosomal integrity across generations. In mammals, this lineage arises from primordial germ cells (PGCs), which are specified early in development and set aside from the pluripotent embryonic cell mass. Following meiosis, these cells directly differentiate into specialized gametes[1]. In flowering plants, the functional equivalent of PGCs are spore mother cells (SMCs), which form later in development within specific floral tissues of the adult organism. In contrast to animal meiotic products, the haploid spores in plants are pluripotent cells that give rise to a multicellular gametophyte, containing several distinct cell types, including the gametes[2]. This difference in timing, tissue origin, and the distinct developmental competence of meiotic products raises important questions about the mechanisms that regulate the de novo specification of SMCs in plants and the establishment of a pluripotent state following meiosis. Specifically, what molecular and cellular factors control the transition from mitotic to meiotic division marking the somatic-to-reproductive fate transition? What controls SMC singleness —ensuring that only one SMC forms per ovule primordium in most species? Understanding these processes is crucial for elucidating how species-specific developmental trajectories and environmental cues influence fertility and yield in flowering plants. Additionally, this knowledge extends to understanding asexual reproduction in plant species that form unreduced spores capable of gametophytic development and clonal seed production. This process called apomixis is highly sought in molecular breeding approaches for agricultural innovation in major crops of interest[3].

Recent studies have uncovered multiple, intricate layers of regulation controlling the establishment of female SMC in the model plant *Arabidopsis*, involving geometrical information, hormonal cues, cell-cell signaling modules, genetic and epigenetic factors[4–10]. Typically, female SMCs are initiated by the enlargement of the most distal cell in the subepidermal layer (L2) of ovule primordia[4,5]. SMC differentiation, defined by distinct morphological features and genetic markers, is a gradual process tightly linked to the growth of the ovule primordium[7]. While the mechanisms controlling the early stages of SMC formation remain not fully elucidated, several non-cell autonomous mechanisms have been identified that govern both SMC formation and singleness. A crucial step in SMC initiation involves the L1 tissue layer, which plays a key role through a mechanism mediated by a transcriptional co-repressor complex, consisting of SPOROCYTELESS/NOZZLE

(SPL/NZZ), which is essential to initiate female SMC development[11] and possibly TOPLESS/TOPLESS-RELATED (TPL/TPR) proteins[12]. This complex likely acts indirectly to enable the expression of *WUSCHEL* (WUS), a homeodomain transcription factor. WUS subsequently activates the expression of *WINDHOSE1* (WIH1) and *WIH2* at the apex of the primordium, which, together with the tetraspanin-type protein *TORNADO2* (TRN2)/EKEKO, contribute to the initiation of SMC formation[4,5,13]. The singleness of SMCs in controlled by lateral inhibitory signals involving small interfering RNAs (siRNAs) and hormones such as auxin and brassinosteroids prevent neighboring cells from adopting an SMC fate[5,8,9,14]. Singleness is also contributed by the growth of the primordium itself whose apex shape likely constrain the domain of action of key regulators alongside direct mechanical cues supporting SMC expansion[7]. Furthermore, the stability of SMC singleness is reinforced by cell cycle regulators, including KIP-RELATED PROTEINS (KRPs), also known as INHIBITORS OF CYCLIN-DEPENDENT KINASES (ICKs), and CYCLIN-DEPENDENT KINASES (CDKs), which help prevent mitotic division of the SMC, by repressing RBR1, an inhibitor of WUS[15,16]. Thus, the acquisition of SMC fate results from the precise spatio-temporal integration of a complex array of intrinsic and extrinsic signals.

Ultimately, SMCs are programmed to undergo meiosis, producing functional haploid spores that give rise to gametes. While the SMC transcriptome has been shown to exhibit signatures of reprogramming[17,18], much remains unknown about the underlying epigenome, which has largely remained inaccessible to detailed study. These changes include the decondensation of heterochromatin, without the loss of epigenetic silencing marks such as H3K9me2, and the loss of several histone variants, including H3.1/HTR13, and H2AZ/HTA11[19,20]. The SMC chromatin becomes also marked by a transcriptionally permissive landscape with the incorporation of the H3.3/HTR5 variant, elevated levels of H3K4me3, acetylation of H4, alongside reduced levels of H3K27me3 and DNA methylation in the CHH context[19,21]. Interestingly, despite these chromatin modifications, overall transcriptional activity remains relatively low in SMCs compared to neighboring cells[19]. Collectively, these large-scale changes in chromatin structure and composition closely resemble those observed in animal PGCs[22] suggesting a possible case of convergent evolution in mechanisms that promote epigenetic reprogramming and establishment of pluripotency in the reproductive lineage[23].

A key event in the chromatin reprogramming of both animal PGCs and plant SMCs is the eviction of linker histones (H1), which precedes large-scale changes in epigenetic marks. In mouse PGCs, somatic H1 subtypes (H1.1–H1.5 and H1.10) are transiently undetectable on chromatin during the early pre-implantation stage (E11.5)[22,24]. Similarly, in *Arabidopsis*, the

canonical H1.1 and H1.2 variants are expressed in ovule primordia and are specifically lost in SMCs at the early ovule primordium stage (stage 1-I)[19]. H1 histones are non-nucleosomal proteins that bind to the nucleosome and linker DNA at the entry or exit points, or both, playing a critical role in promoting spatial proximity between nucleosomes and facilitating chromatin fiber compaction. While long considered to serve only a structural role in chromatin folding and often viewed as hindering transcription, recent studies have uncovered a more complex interaction between H1 histones and epigenetic regulation, including DNA methylation, histone methylation, and acetylation, both in plants and animals[1–7]. This raises the question of whether the loss of H1 at the somatic-to-reproductive transition is a key regulatory event that controls cellular reprogramming in both plant SMCs and mouse PGCs. Supporting this hypothesis, the H1 depletion in mouse PGC is critical for establishing pluripotency within the germline[25]. Similarly, H1 depletion in mouse embryonic stem cells leads to the upregulation of pluripotency genes, causing the cells to stall in a self-renewal state with impaired differentiation potential[26].

In *Arabidopsis*, the role of H1 eviction in the SMC remains unclear, particularly regarding its potential influence on sporogenesis, meiosis, gametogenesis, or a combination of these processes. To investigate this, a strategy to prevent H1 eviction is required. Previous attempts to overexpress H1 variants using strong, ubiquitous promoters did not result in ectopic H1 expression in the SMC (Baroux, unpublished). Therefore, we employed a series of hypothesis-driven approaches to conditionally block the H1 eviction process specifically in the SMC. Through this, we demonstrate the involvement of a proteasome-mediated degradation mechanism, with the E3 ligase CULLIN4 playing a key role, and we pinpoint a specific lysine residue as potential ubiquitination site for H1.1 in the SMC. Additionally, we show that the plant citrullinase AIH plays a critical role in regulating H1 stability, with a single arginine residue identified as a likely target for citrullination. Based on these findings, we propose citrullination as a mechanism destabilizing H1.1, exposing it to ubiquitination and further degradation in the SMC. Importantly, our results show that disrupting H1 eviction in the SMC does not affect SMC differentiation or meiosis directly. However, it compromises gametogenesis ultimately resulting in sterility. Collectively, our work provides new evidence for a pre-meiotic chromatin reprogramming event relying on H1 eviction contributing to post-meiotic fate.

Results

H1.1 degradation in the SMC is mediated by the E3-ubiquitin ligase CULLIN4

We previously showed that H1.1 and H1.2 depletion from the SMC chromatin was dampened in presence of the proteasome inhibitor Syringolin A[19]. Because ubiquitin-mediated targeting to the proteasome is a major pathway for protein degradation in plants[27] we thought to investigate the role of E3 ligases of the CULLIN family resuming the cascade of ubiquitin transfer to the target protein[28]. Specifically, available data indicated that *CULLIN4* is expressed in young ovule primordia[29] and notably in female SMC (**Figure S1A**). We rationalized that if CULLIN4 is involved in H1 degradation, its downregulation at the onset of ovule primordium development should lead to the maintenance of linker histones in mature SMC. We thus designed an artificial microRNA targeting *CULLIN4, amiR[CUL4]* (**Figure S1B**), and expressed it under the control of the *pOP/LhGR* Dexamethasone (Dex)-inducible system, where the transactivating factor LhGR is driven by the RPS5a promoter[30,31], in an H1.1-GFP expressing reporter line (*pH1.1::H1.1-GFP*[19]). As a control, we induced *amiR[CUL4]* expression in seedlings and observed a known *CUL4* loss-of-function phenotype[29] and reduced CUL4 protein levels (**Figure S1C, D**). We then induced *amiR[CUL4]* expression in young flower buds and scored ovule primordia stage 1-II/2-I five days post induction (5 DPI) showing H1.1 eviction, or persistence, in the SMC (see Methods and[32]). *CUL4* downregulation led to the persistence of H1.1-GFP in SMCs at high frequency compared to the Mock control (52%, n=178 vs 11%, n=137, $P<0.001$, **Figure 1A**), similarly to primordia treated with the proteasome inhibitor epoxomicin (**Figure 1B**). Collectively, our results indicate that the E3-ubiquitin ligase CULLIN4 plays a role in H1.1 degradation during SMC development.

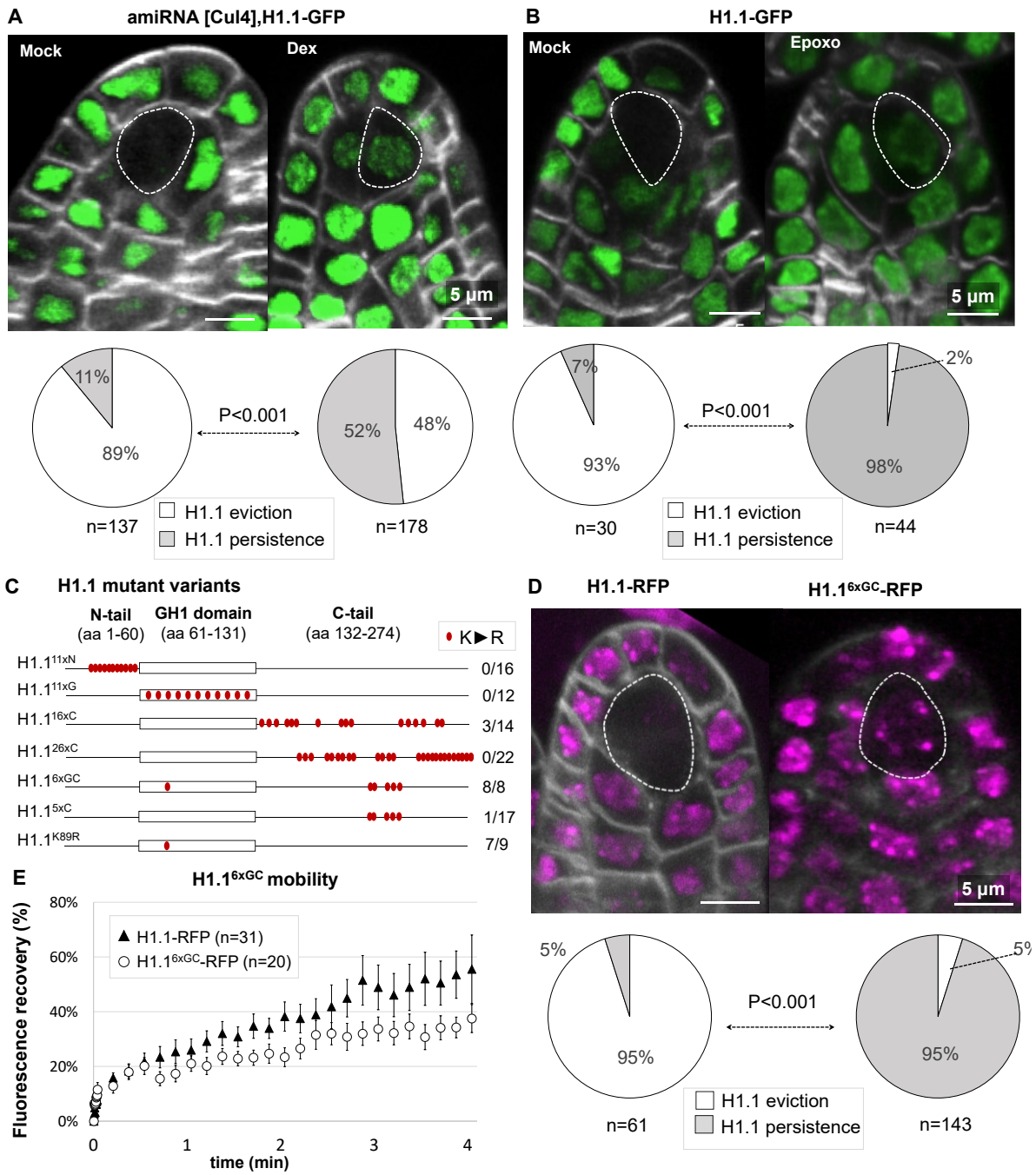

Figure 1 H1.1 degradation is mediated by the E3-Ubiquitin ligase CULLIN 4

(A-B) H1.1-GFP degradation in the SMC is impaired when inducing the expression of an artificial miRNA against *CUL4* (**A,** *amiRNA[CUL4]*) or when treating with the proteasome inhibitor epoxomycin (**B**). Young inflorescences were treated either with 10µM dexamethasone or a mock solution as control (A, Dex, Mock) [30,31] , or with a 5µM epoxomicin solution or mock solution as control (B, Epoxo, Mock). Images shows partial projections of confocal images showing the GFP signal (green) and cell wall stained with Renaissance[33] (grey). The SMC is indicated with dotted contours. Pie charts below the images show the proportion of ovule primordia at stage 2-I/2-II 5 days post induction (5dpi) showing either H1.1-GFP eviction (white) or persistence (grey) in the SMC. n, number of primordia scored. P value from a Fischer-exact test. Replicate experiments in Supplemental data 1, scoring data in Data Source 1. **(C)** Schematic representation of H1.1 mutant variants carrying several K-to-R amino acid substitutions (red dots) in their N-terminal tail, globular domain, C-terminal tail, or a combination thereof, and fused to RFP. The numbers on the right indicate the number of independent lines showing a persistent signal in the SMC, indicating a lack of degradation, over (/) the total number of lines

screened. (**D**) Representative images of H1.1-RFP and H1.1^{6xGC}RFP expression in ovule primordia at stage 2-I, 5dpi. Pie charts show the proportion of ovule primordia showing either H1.1-RFP eviction (white) or persistence (grey) in the SMC. n, number of primordia scored. P value from a Fischer-exact test. Replicate experiments in Supplemental data 1, scoring data in Data Source 1. **(E)** Fluorescence recovery after photobleaching (FRAP) of H1.1-RFP and H1.1^{6xGC}RFP in root nuclei from 5 days old seedlings grown in Dex. n, number of analyzed nuclei. Statistical analysis in Figure S1, raw data in Data Source 1.

A screen for potential ubiquitination targets identifies K89 as an important lysine in the globular domain of H1.1

E3-ligases target preferentially lysine- rich regions[28]. Given that linker histones are particularly rich in lysine throughout their protein sequence[34], we addressed the possibility that ubiquitination of one or several lysines drive H1 degradation. To test this hypothesis, we first created six H1.1 mutant variants with batches of K-to-R amino acid substitutions (**Figure 1C**). Candidate lysine targeted for creating H1.1 variants, were selected based on computational predictions[35–37], proteomic evidence of ubiquitination in seedling tissues[37] and comparison with ubiquitinated sites in mouse and human counterparts[38]. These H1.1 variants were designed to carry K-to-R mutations in the N-terminal domain, the Globular domain, the C-terminal domain or a combination thereof, and were expressed as RFP translational fusions under the control of the Dex-inducible pOP/LhGR system[30,31]. We induced and screened primary transformants for H1.1-RFP depletion versus persistence in the SMC of ovule primordia collected at 5DPI as before. Of all six variants, only one, named H1.1^{6xGC}, showed a strong persistence of H1.1 in the SMC in all T1 lines screened (**Figure 1C**). This H1.1 variant was mutated in all 6 sites shown to be ubiquitinated in seedling tissues, including one residue in the globular domain and five in the C-tail[37], (**Figure S1E**). Typically, 76-95% ovule primordia expressing H1.1^{6xGC}-RFP showed a clear signal in the SMC at stage 2-I (**Figure 1D** and **Figure S1E** for replicates). In contrast, primordia expressing a native H1.1 variant fused with RFP (H1.1-RFP) under the control of the same Dex-inducible system, showed depletion in the SMC in 95% ovule primordia at stage 2-I (**Figure 1D**), with the remaining 5% showing only weak, residual signals. This could suggest either an enhanced, electrostatic, stability of H1.1^{6xGC}-RFP on the chromatin, a lack of targeted degradation, or a combination thereof. To answer this question, we used Fluorescence Recovery After Photobleaching (FRAP), which allows us to measure the mobility of (tagged) H1 variants in vivo, and was shown a powerful approach to determine the contribution of specific H1 sites in binding the nucleosome[39]. Here, we compare the recovery rates of H1.1-RFP and H1.1^{6xGC}-RFP following photobleaching in dexamethasone (Dex)-treated seedling root nuclei. The data indicates a similar mobility, both during the initial,

rapid recovery phase and later, during the slow recovery phase (**Figure 1E; Figure S1G**). This suggests that the conversion of six lysines into arginines did not enhance H1.1 stability, which is consistent with the predicted ionic charge conservation. Instead, considering the observation that these lysines can be ubiquitinated in seedling tissues, our findings strongly suggest that these K-to-R mutations might disrupt a ubiquitination-dependent degradation pathway.

To further distinguish the contribution of the different lysine mutated in the H1.1^{6xGC} variant, we created two additional mutant variants: one carrying a single mutation at lysine 89 (K89R) in the globular domain (H1.1^{K89R}) and one variant with K-to-R mutations at the 5 remaining lysines in the C-terminal tail (H1.1^{5xC}, **Figure 1C**). We expressed them under the control of the Dex-inducible system and screened several independent transformants as before. The recapitulation of the persistence phenotype in 7 of the 9 lines expressing H1.1^{K89R}-RFP but in none of 16 lines expressing H1.1^{5xC}-RFP (**Figure 1C, Figure S1I**) indicates that K89R alone is responsible for H1.1 persistence in the SMC chromatin (**Figure S1J**). This lysine, exposed at the surface of the third alpha-helix of the globular domain (**Figure S1H**) is conserved across several H1 variants but does not seem to contribute significantly to interactions with the nucleosome, as shown for the mouse MmH1(o) variant where a mutation at K52, equivalent of K89 in AtH1.1, did not change H1(o) mobility[39]. Similarly, the K89R mutation in the *Arabidopsis* H1.1 variant did not affect the overall mobility of H1.1 (**Figure S1G**). Finally, we observed that both H1.1^{6xGC}-RFP and H1.1^{K89R}-RFP showed a nuclear distribution similar than the native H1.1-RFP, present in both euchromatin and heterochromatin (**Figure SI1I**).

In conclusion, we identified a conserved lysine residue, K89, in the globular domain of H1.1 that plays a key role in the degradation of H1.1 within the SMC. The fact that this lysine does not affect binding affinity and can be ubiquitinated in seedlings strongly supports a model in which ubiquitination at K89, likely contributed by CUL 4, drives H1.1 degradation. Whether CUL4 directly or indirectly on H1.1 remains to be determined.

A single arginine residue in the N-terminal tail controls H1 eviction in the SMC

Ubiquitin-mediated protein degradation is a basic cellular process and CUL4 is expressed throughout the ovule primordium[40]. Hence, we wondered whether another post-translational modification (PTM) of H1.1 might prime H1.1 for ubiquitination in the SMC. Interestingly, H1.2 eviction in mouse PGCs[22] is controlled by citrullination of R52, a PTM consisting in the conversion of an arginine into citrulline[25]. We thus wondered whether a similar citrullination

mechanism might operate in the control of H1.1 eviction in *Arabidopsis* SMCs. We created RFP-tagged H1.1 variants either with a lysine substitution at R57 (R57K) that ensures charge conservation, or an alanine substitution (R57A) which mimics the neutral charge of the citrulline (**Figure 2A**). We expressed it under the control of the *pOP/LhGR Dex*-inducible system and analyzed the presence / absence of H1.1 in the SMC of ovule primordia as before. While the H1.1^{R57K}-RFP variant showed a persistent signal in a consistent fraction of primordia, the H1.1^{R57A}-RFP variant showed a similar proportion of SMC with clear eviction as in the wild-type H1.1-RFP control (**Figure 2B** and **Figure S2A**). The R57K mutation also compromised H1.1 depletion from the chromatin of male SMCs, whereas the R57A mutation did not (**Figure S2B**).

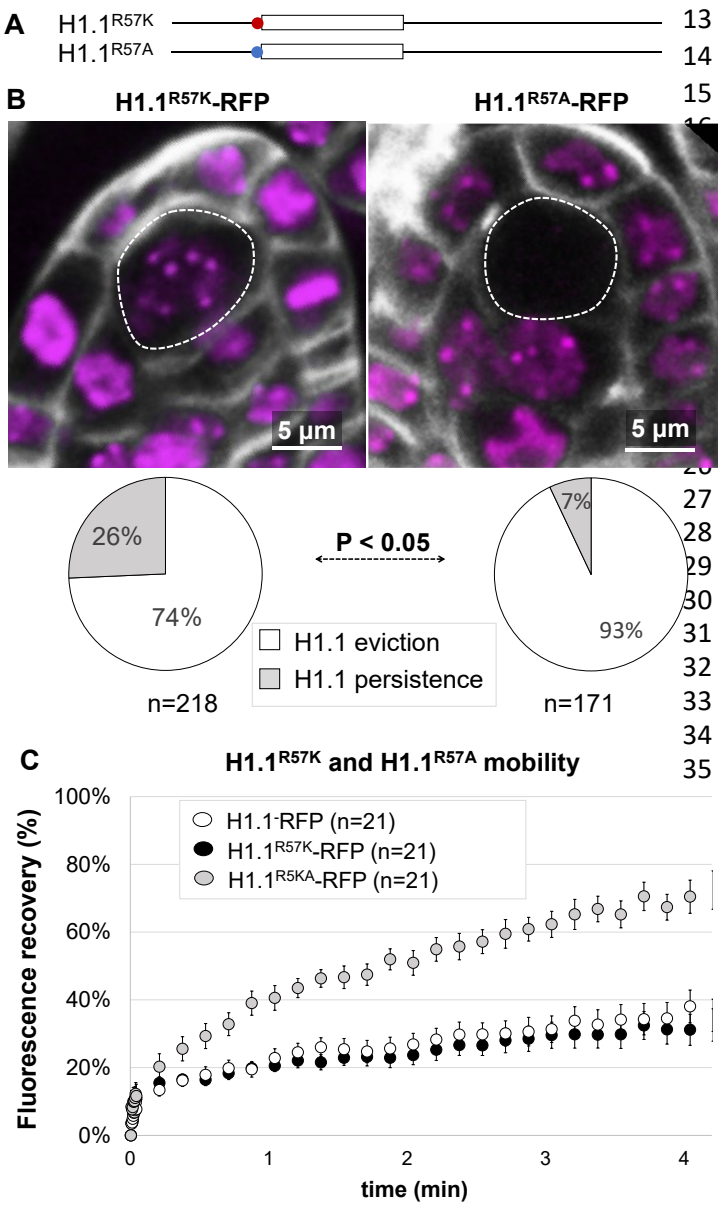

Figure 2. An R57K substitution prevents H1.1 eviction in SMC without affecting H1.1 mobility.
(A) Schematic representation of the R57K and R57A mutation just before the globular domain (**B**) Representative images of H1.1^{R57K}-RFP and H1.1^{R57A}-RFP in ovule primordia stage 2-I at 5dpi, showing persistence and eviction in the SMC (dotted lines), respectively (partial z-projections; RFP: magenta; Renaissance: grey). Pie charts below show the proportion of ovule primordia showing H1.1(mutant)-RFP eviction or persistence in the SMC. n, number of primordia scored. P value: Fischer exact test. Replicate experiments in Figure S2. **(B)** Fluorescence recovery after photobleaching (FRAP) of H1.1-RFP, H1.1^{R57K}-RFP and H1.1^{R57A}-RFP in root nuclei from 5 days old, Dex-induced seedlings. n, number of nuclei. See also Figure S2 and Data Source 2.

To assess whether the persistence of H1.1^{R57K}-RFP in the SMC is due to enhanced chromatin stability compared to H1.1^{R57A}-RFP or H1.1-RFP, we conducted FRAP analyses as previously described. Notably, the R57K mutation did not affect H1.1 mobility, whereas the R57A mutation significantly increased it, as evidenced by a two-fold increase recovery rate (**Figure 2C, Figure S2C**). Since the stability of linker histones binding to the nucleosome is primarily governed by electrostatic interactions involving positively charged amino acids[39,41], the most likely explanation is that the alanine substitution caused charge neutralization, weakening the electrostatic interactions between H1.1 and chromatin. This disruption likely led to a reduced residency time and, as a result, a faster recovery rate.

Of note, while R57 in the *Arabidopsis* H1.1 variant is conserved in the mouse H1.2 variant (R32), the actual homologous residue of R52 in the mouse H1.2 variant described in Christophorou and colleagues[25] is R79 in the *Arabidopsis* H1.1 variant, located just at the beginning of the globular domain (**Figure S2C**). Future work will thus have to clarify whether R79 also contributes to H1.1 dynamics.

AIH, a candidate arginine deiminase is necessary for H1.1 eviction.

The observation that the R57K mutation prevents H1.1 eviction, whereas the R57A mutation does not, suggests that the effect may not be due to a classical biochemical modification of arginine, such as methylation. Instead, the fact that charge neutralization impacts H1.1 stability points to citrullination as a prime candidate mechanism. Citrullination driven by peptidyl arginine deiminases such as PADI enzymes in animal cells, results in the net loss of a positive charge and has previously been shown to play a role in H1.2 eviction in mouse PGCs[25]. Although the *Arabidopsis* genome does not encode proteins fully homologous to PADI enzymes, a 3D protein structure homology search identified AGMATINASE IMINOHYDROLYASE (AIH) as closely related to the catalytic domain of PADI4, with a striking conservation of the four key catalytic amino acids (**Figure 3A**). AIH is predicted to be expressed in young flower buds stage 8-10 according to publicly available transcriptome datasets[42], (**Figure S3A**) and has been shown to exhibit citrullinase activity *in vitro*[43]. Using RNA *in situ* hybridization, we further confirmed that *AIH* is expressed in young ovule primordium including in all apical L2 cells and in the SMC (**Figure 3B**, **Figure S3B**). To test whether AIH might play a role in H1.1 eviction we induced the expression of an artificial miRNA against *AIH* (*amiR[AIH]*, **Figure S3C**) using the Dex-induction system as before in an H1.1-GFP expressing line. In line with our hypothesis, H1.1-GFP eviction in the SMC was

impaired when *amiR[AIH]* was induced compared to mock-treated tissues, with 37% and 6% ovule primordia showing H1.1 persistence (n=30 and n=47), respectively (**Figure 3C** and **Figure S3D**). To test the involvement of AIH independently, we used Cl-amidine, a known inhibitor of the mammalian citrulinase PADI4 which binds the catalytic domain[44] highly conserved in AIH (**Figure 3A**). Cl-amidine treatment indeed prevented H1.1 eviction in the SMC of a large fraction of ovule primordia (39%, n=56) compared to the mock treatment (**Figure 3D** and **Figure S3E**).

In conclusion, genetic and toxicological evidence support a model involving AIH as a candidate citrulinase of H1.1 contributing its eviction in SMC.

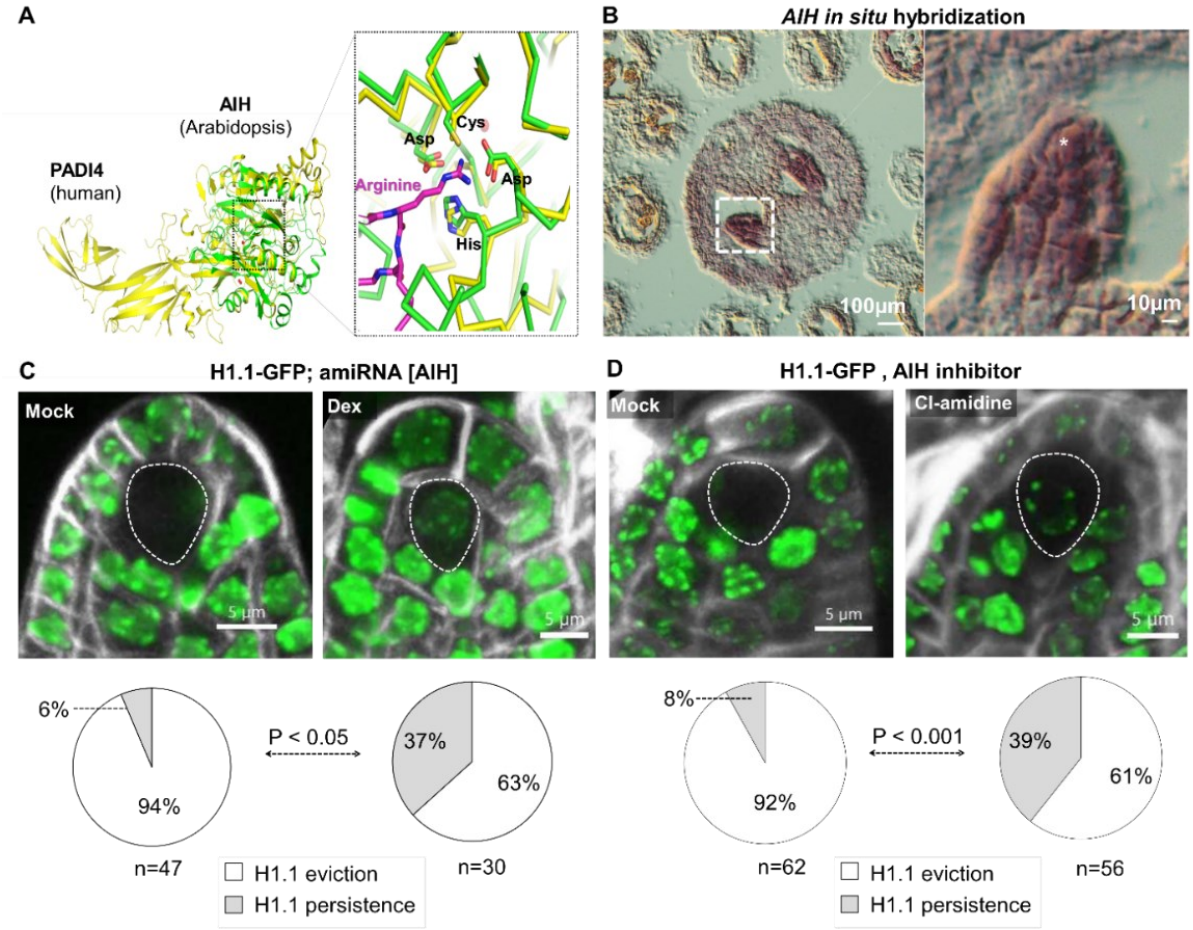

Figure 3 Citrullinase AIH Downregulation Impairs H1.1 Eviction in SMC

(A).3D protein structure of the human citrullinase PADI4 (yellow, PDB model 2DEW) and the *Arabidopsis* citrullinase AIH (green, PDB model 1VKP) showing structural homology of AIH with the catalytic head of PADI4 and a perfect conservation of the catalytic site (Asp, Cys, Asp and His, inlet). **(B)**. Histochemical detection of *AIH* transcripts following RNA *in situ* hybridization on a transversal section of a flower bud stage 10 (left) revealing a specific signal in ovule primordia (box in dashed line and zoomed-in image on the right). **(C,D)** H1.1-GFP eviction in the SMC is prevented when inducing the expression of a downregulating artificial miRNA against *AIH* (*amiRNA[AIH]*, Dex versus mock, C) or when treating with the PADI4-specific enzyme inhibitor Cl-amidine (D). Images show partial projections of confocal images showing the GFP signal (green) and Renaissance cell boundary staining

(grey). Pie charts below the images show the proportion of ovule primordia 5 dpi harboring no or persistent H1.1-GFP signal in the SMC. n, number of primordia scored. P value from a Fischer exact test. Replicate experiments in Figure S3, Data Source 3.

H1 persistence in the SMC affects chromatin reorganization without impairing SMC maturation or meiosis.

Next, we asked the question whether the persistence of H1.1 in the SMC would affect chromatin reorganization as shown previously[19]. We chose to analyze key markers of constitutive and facultative heterochromatin that were shown to decrease during the SMC chromatin transition[19,21]: the relative heterochromatin fraction comprised in chromocenters (RHF), the levels of the LHP1-GFP reporter as a reader of H3K27me3[45], and the levels of the mCHH-Venus reporter as a reader of methylated DNA in the CHH context[21]. SMC expressing a persistent H1.1 variant, because of the R57K mutation, showed higher levels of all of these heterochromatin markers compared to SMC that lost the native H1.1 or H1.1^{R57A} mimic variant (**Figure 4A-C**). Yet, H1.1 persistence due to lysine substitutions as in the H1.1^{6xGC} variant did not show significant changes for these markers compared to the control (**Figure C**, **Figure S4A-B**). One possibility to explain this observation is that the H1.1^{6xGC} variant bearing an intact R57 residue is citrullinated hence gain a higher mobility, with shorter residency time on the chromatin, which might be sufficient to enable heterochromatin decondensation and downstream events regulating H3K27me3 levels.

We then asked whether the persistence of H1.1 would affect SMC differentiation and meiosis. First, we assessed SMC growth and the expression of the fate marker *KNU::nlsYFP*, two hallmarks of SMC maturation[20,46]. We found that preventing H1.1 eviction because of either mutation compromised SMC growth, as revealed by a 3D analysis of the primordium (**Figure 4D, Figure SC**). In contrast, the size of companion cells increased (**Figure SD**). Yet, *KNU::nlsYFP* expression was not altered in ovule primordia expressing either of the H1.1 mutant variant **(Figure 4E)**. Next, we assessed meiosis by scoring primordia expressing the marker ASY1-YFP loaded at prophase I[47] and the occurrence of tetrads. Ovule primordia induced for the expression of either H1.1 mutant variant showed a normal occurrence of these meiotic markers, like in the control (**Figure 4F-G**). The large companion cells observed in premeiotic ovule primordia persisted at the tetrad stage (**Figure S4E**).
Our results thus indicate that impairing H1.1 eviction in SMCs moderately affects heterochromatin reorganization and SMC growth but does not interfere with meiosis execution.

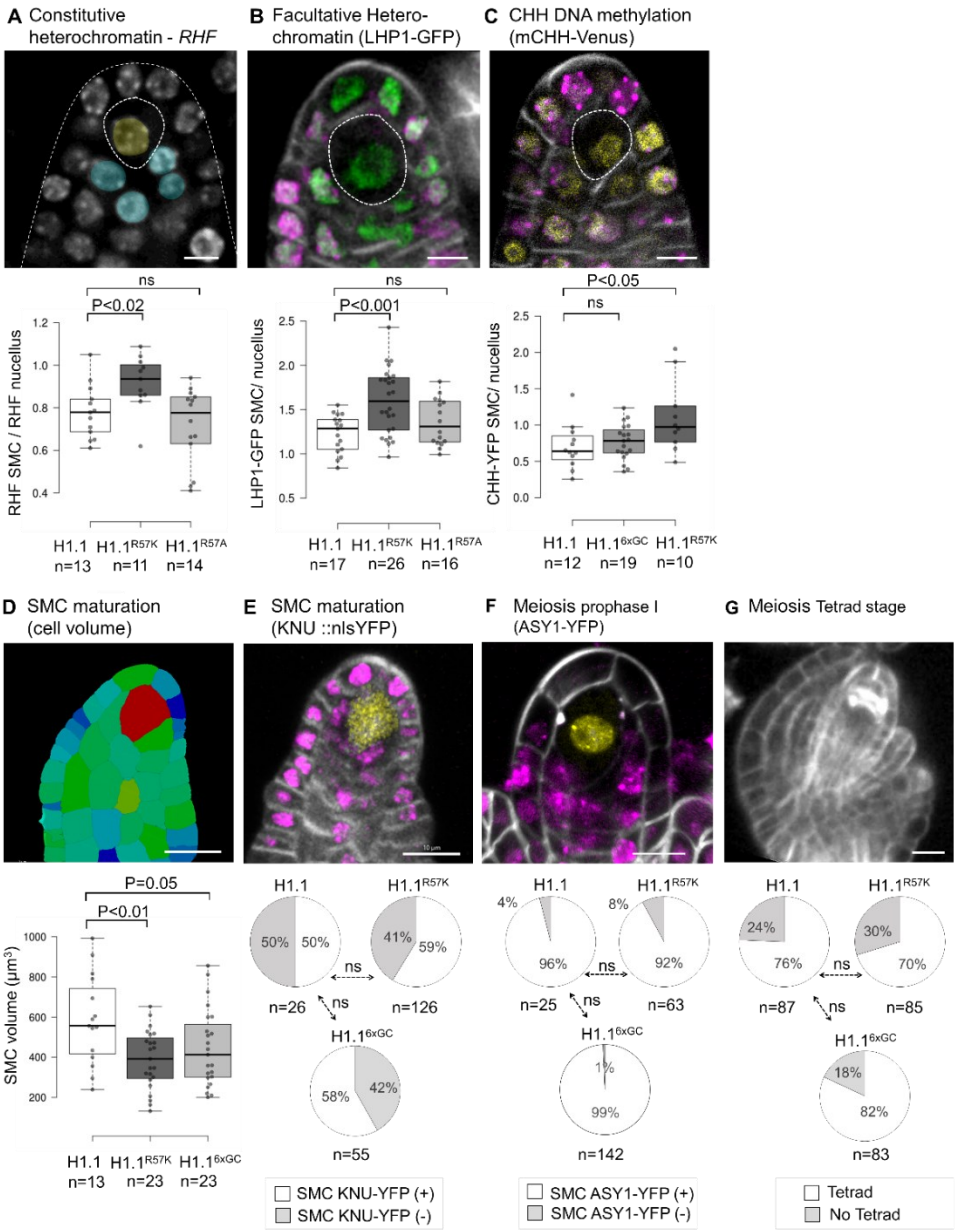

Figure 4 Inhibition of H1.1 eviction in the SMC disrupts chromatin reorganization without affecting meiosis

(A-C) Quantification of heterochromatin markers in the SMC of ovule primordia stage 2-I/2-II at 5dpi in lines expressing H1.1-RFP, H1.1^{R57K} -RFP, H1.1^{R57A}-RFP or H1.1^{6xGC}-RFP (H1.1, H1.1^{R57K}, H1.1^{R57A}, H1.1^{6xGC}, respectively). Top: representative images (confocal projections) in H1.1-RFP control lines following whole-mount propidium iodide (PI) staining (A, yellow: SMC; blue: nucellus nuclei used as references); live GFP (B, green), YFP (C, yellow), RFP (B, C, magenta) and Renaissance counterstaining (B-C grey); Bottom: Graphs showing the relative heterochromatin fraction (RHF) in chromocenters (A), and relative LHP1-GFP (B) and mCHH-Venus (C) intensity in the SMC. The measurements are expressed relative to the nucellus. **(D-G)** Quantification of SMC maturation in ovule primordia stage 1-II/2-I at 5dpi (D, E) and meiosis markers in ovule primordia stage 2-III/3-I at 7dpi (F, G) in lines expressing H1.1-RFP, H1.1^{R57K} -RFP, H1.1^{R57A}-RFP, indicated above the pie charts as in A-C. Note that due to the progressive and variable expression of the KNU::nlsYFP , not all primordia showed a detectable signal also in the wild-type control. Top: representative images in the H1.1-RFP control line following: Renaissance staining, 3D imaging and cell segmentation with cells colored according to their volume (D), live imaging of KNU::nlsYFP (E, yellow), ASY1-YFP (F, yellow), H1.1-RFP (E-F, magenta), Renaissance counterstaining (E-G, grey) and confocal imaging (partial

projection shown). Scale bars: 5µm (A-C), 10µm (D-G). P values, Mann-Whitney U test (A-D), Fisher exact test (E-G). n, number of ovule primordia.

Inhibiting H1.1 eviction in the SMC impairs gametogenesis.

Female meiosis results in the production of four haploid spores, three of which degenerate. The surviving spore enlarges to become the functional megaspore (FM), which will develop into the female gametophyte, or embryo sac, through endomitosis followed by cellularization to form the egg cell and the central cell along with accessory cells[2]. Given that SMC expressing the H1.1 mutant variants did not impact meiosis, we next asked whether FM derived from SMC expressing either of the H1.1 mutant variants were properly differentiated (7dpi) and able to develop a mature embryo sac (9dpi). The FM-specific marker, *AKV::H2B-YFP,* consisting in a fluorescent H2B reporter driven by the *ANTIKEVORKIAN* (*AKV*) promoter[17,48], was scored at similar frequency in wild-type and mutant ovules (**Figure 5A, Figure S5A**). Embryo sac (ES) development, however, seemed compromised, with a high proportion of Es at stages FG2-FG4 in both mutant variants whereas the control harbor a majority of mature ES at stage FG6 (**Figure 5B, Figure S5B**). To determine whether this was due to developmental arrest or a delay, we emasculated flowers at 9dpi and allowed them to develop further, re-analyzing them at 11dpi. Interestingly, in lines expressing the H1.1^{R57K} variant, the proportion of mature ES at 11dpi was no longer different than in the control line (**Figure 5B**) suggesting that the abnormal ES initially detected at 9dpi were delayed rather than aborted. The same observation was made in *amiR[AIH]* expressing lines showing a large fraction of delayed ES at 9dpi rescued at 11 dpi (**Figure S5C**). In contrast, a large proportion of abnormal ES persisted in the H1.1^{6xGC}-expressing lines (**Figure 5B, Figure S5B**) indicating a distinct functional impact of this variant compared to H1.1^{R57K} discussed below. Finally, we assessed seed fertility in mature siliques produced 20 days post induction of flower buds for either of the mutant or control variants. The H1.1^{R57K} and H1.1^{6xGC} expressing lines exhibited a significantly higher rate of seed abortion (about 50%) compared to the control line (**Figure 5C**) Although these lines harbored a large amount of aborted pollen (**Figure S5D**), a significant proportion of viable pollen remains. Hence the high rate of infertile ovules suggests failure at fertilization and requires further analysis. Additionally, induction of *amiR[AIH]* and *amiR[Cul4]* in the same conditions as before resulted in high sterility compared to mock controls (**Figure S5E**). Yet, at least for the *amiR[Cul4]* line, this might be partly attributed to the misregulation of multiple targets, as observed in the *CUL4* loss-of-function mutant [40].

In conclusion, blocking H1.1 eviction in the SMC, caused by either the R57K or 6xGC mutations, influences mitotic progression during embryo sac development. Notably, the two mutant variants exhibited distinct effects. The H1.1^{R57K} variant, which cannot undergo citrullination, showed partial developmental recovery when flowers were left for two additional days post-emasculation. In contrast, the H1.1^{6xGC} variant, which can be citrullinated but not degraded, displayed no recovery, highlighting how these mutations differently affect the chromatin state prior to meiosis. This suggests that H1.1 eviction in the SMC is essential for post-meiotic development.

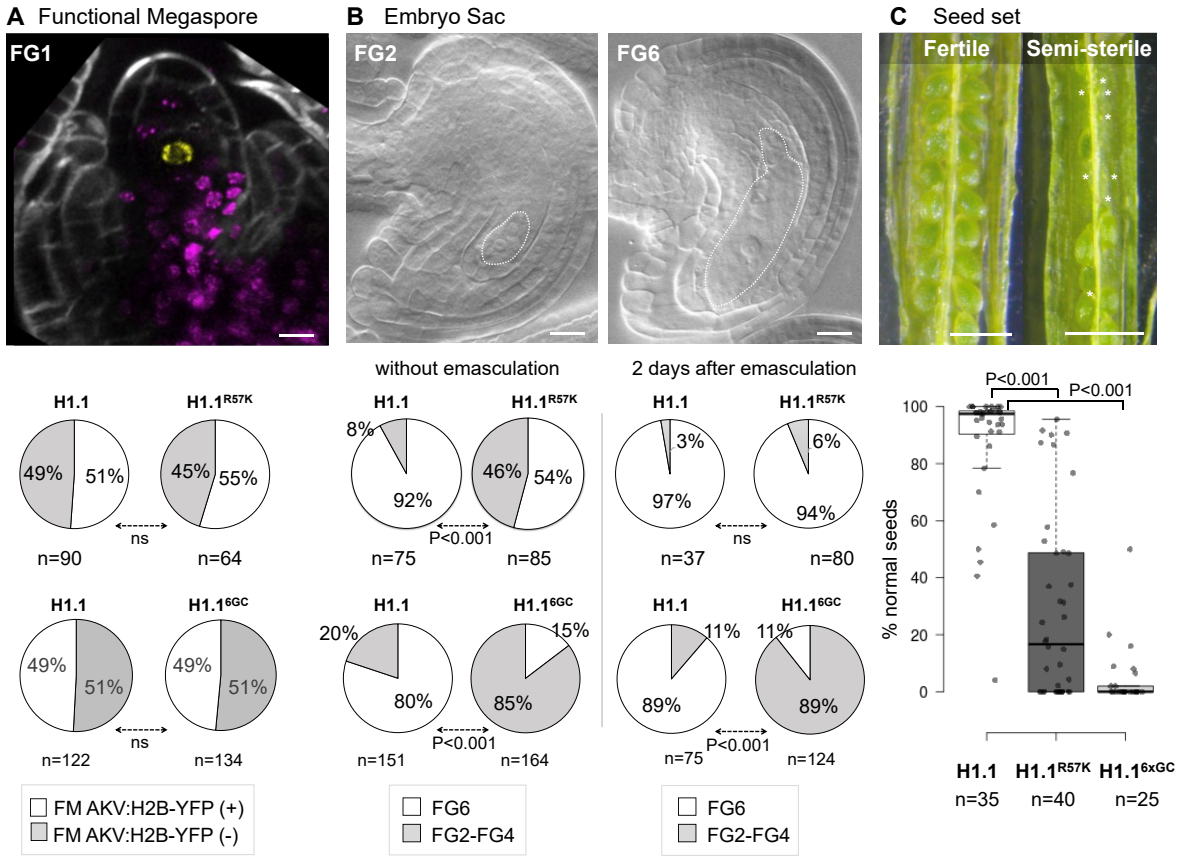

Figure 5. H1.1 persistence in the SMC impairs gametogenesis

(A-B) Analysis of functional megaspore (FM) fate establishment and embryo sac development in ovules derived from primordia induced for the expression of the H1.1^{R57K}-RFP and H1.1^{6xGC}-RFP persistent variants or the H1.1-RFP control variant. Representative images of an ovule at the FG1 stage counterstained with Renaissance (grey) expressing the functional megaspore-specific marker, *AKV::H2B-YFP* [17](yellow) and H1.1-RFP (magenta) at 7dpi (A) and of cleared ovules at the FG2 and FG6 stage showing a 2-nucleate and a mature embryo sac, respectively at 9dpi (B) with respective scoring in F1 plants showing segregation of *AKV::H2B-YFP* (pie charts below) of the functional megaspore marker occurrence at 7dpi (A) or of mature embryo sacs (FG6) vs earlier stages (FG2-FG4) in ovules at 9dpi without emasculation or at 11dpi and after emasculation as indicated. Scoring for each mutant variant-expressing lines was compared to the control line in independent experiments. Slight differences in ovule development progression at the time of flower bud collection between experiments explain the different frequencies of AKV::H2B-YFP expression between replicates scoring in the control line. n, number of ovules scored. P values from a Fisher exact test. Scale bar, 20 µm. **(C)** Seed set analysis in siliques 20dpi derived from flower buds stage 9 induced for H1.1-RFP, H1.1^{R57K}-RFP

and H1.1^{6xGC} -RFP expression. Representative images of a fully fertile silique (H1.1-RFP control line), and semi-sterile stilique (H1.1^{R57K}-RFP mutant line) at 20dpi and scoring of normal seeds (plots) for all three genotypes as indicated.*, infertile ovules. n, number of siliques scored (ca 50 seeds p. silique). P values, Mann Whitney U test. Scale bar: 1mm. See replicate measurements Figure S5 and raw data in Data Source 5.

DISCUSSION

The eviction of canonical H1 linker histones is a hallmark of the somatic-to-reproductive fate transition in both plants and animals[19,22]. In mice, H1.2 eviction from the PGCs is critical for establishing pluripotency [25]. In the flowering plant *Arabidopsis*, the loss of H1.1 and H1.2 in male and female spore mother cells (SMCs) precedes extensive chromatin reorganization involving both structural alterations and epigenetic modifications[19,49] but neither the mechanisms nor the functional implication of H1's removal were known.

A citrullination-ubiquitination model for premeiotic H1.1 eviction in female SMCs

Previously, we proposed that the loss of H1.1 in the SMC occurs through proteasome-mediated protein degradation[19]. Plants possess several pathways for protein degradation but ubiquitin-mediated protein degradation is prevalent [27,50]. Protein ubiquitination involves an enzymatic cascade where ubiquitin is transferred from the E1 ubiquitin-activating enzyme to the E2 ubiquitin-conjugating enzyme, and ultimately to the target protein, either directly or indirectly through an E3 ubiquitin ligase[51]. In this study, we demonstrate a role for CUL4 in H1.1 degradation in the SMC, extending its previously reported functions in DNA replication, repair, and chromatin remodeling[52]. Whether CUL4 acts directly or indirectly on H1.1 for instance via the formation of a CUL4 RING ligase (CRL4) complex remains to be determined. CRL4s share multiple roles in the nucleus, including processes affecting chromatin states[53]. Interestingly, in rice, a CRL4 complex has been shown to ubiquitinate the Argonaute protein MEIOSIS ARRESTED AT LEPTOTENE1 (MEL1), leading to its degradation prior to meiosis[54]. This clearance of MEL1 is essential for the progression of meiosis and the formation of viable microspores.

Here, to identify the H1.1 regions possibly targeted for ubiquitination, we engineered several mutant variants with modifications at one or more candidate lysine in the N-tail, the globular domain (GH1) or the C-tail. Whereas substituting several lysine for arginine in the N- and C-tails did not affect H1.1 dynamics in the SMC, the H1.1^{6xGC} variant, where five lysine in the C-terminal domain and one in the globular domain were substituted, showed protection from degradation. Interestingly, this protection was not due to an increased binding affinity to

chromatin, as the mobility of this mutant was similar to that of the native variant in vivo. Further variants pinpointed K89 as the critical residue responsible for H1.1 degradation. Whether K89 is the direct target of CUL4 in the SMC remains to be formally demonstrated. Currently, co-immunoprecipitation and mass spectrometry techniques are not feasible for such an analysis. However, the detection of H1.1-K89Ub in leaves[55] supports our model, suggesting that CUL4 may indeed mediate H1.1 degradation through K89 ubiquitination.

Intriguingly, a mutated H1.1 variant ($H1.1^{11xG}$, Figure 1) with 11 lysine substituted residues in the GH1 domain including the K89R mutation, exhibited normal eviction in the SMC across twelve independent transformants. Sequencing confirmed the presence of all substitutions in the introduced construct (data not shown). While this suggests that K89's role in degradation requires an intact GH1 domain, it is unlikely that the 11 K-to-R substitutions disrupt GH1 folding, as the latter is highly resilient to amino acid changes[41]. At present we cannot fully explain this observation but suggest that H1.1 degradation might be subject to versatile and redundant mechanisms involving concurrent or cooperative PTMs. In support of this hypothesis, H1.1 in leaves was found to carry a variety of PTMs, including crotonylation at six lysines [56].

Furthermore, our findings indicate that another, upstream PTM is necessary for efficient H1.1 eviction: indeed, parallel efforts to identify key regions involved in H1.1 dynamics pinpointed R57 as a critical residue. Substituting R57 with a lysine ($H1.1^{R57K}$) protects H1.1 from degradation in the SMC, suggesting that the K89 residue in $H1.1^{R57K}$ alone is insufficient for degradation. In contrast, an intact R57 residue is essential for this process. Notably, the $H1.1^{R57A}$ mutant is degraded in the SMC, but this degradation is blocked when combining the R57A mutation together with the 6xGC modifications that include the K89R mutation ($H1.1^{R57A,\ 6xGC}$, **Figure S6**). A key observation is the increased mobility, ie lower stability on the chromatin, of the $H1.1^{R57A}$ mutant variant. This suggests a two-step, destabilization-degradation model (**Figure 6**) in which charge neutralization, notably at R57, destabilizes electrostatic interactions between H1.1 and the nucleosome. This weaker interaction is expected to reduce residency time on chromatin that, in turn, increases the proportion of unbound H1.1 exposed to CUL4 for ubiquitination and subsequent targeting to the proteasome.

Supporting this model, we identified AIH, a plant citrullinase that catalyzes the deimination of arginine, as critical for H1.1 eviction in the SMC. These findings are reminiscent of the work of Christophorou and colleagues[25] who demonstrated that citrullination of H1.2 at R54

promotes its eviction in PGCs. In this model, the deimination of arginine to citrulline results in a net loss of a positive charge, reducing H1.2's binding affinity to the nucleosome. Although the degradation mechanism of the destabilized protein was not explored in their study, it would be interesting to investigate whether a similar ubiquitin-mediated degradation pathway operates in mouse PGCs.

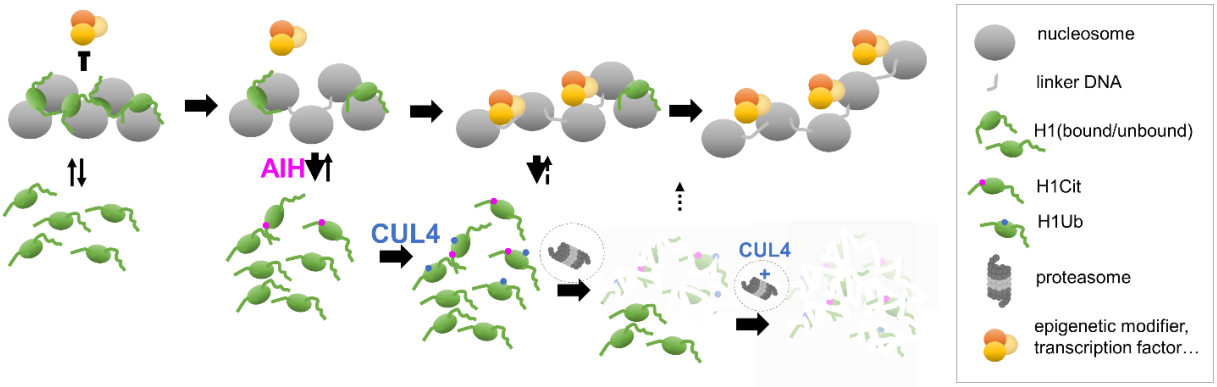

Figure 6. A two-step destabilization-degradation model of H1.1 eviction in the SMC
Based on our findings, we propose a two-step model explaining the depletion of H1.1 from the SMC chromatin. First, H1.1 is electrostatically destabilized due to charge neutralization by the citrulinase AIH, particularly at residue R57, while other target residues are not excluded. This process increases the pool of unbound proteins, making them susceptible to ubiquitination by CUL4 and subsequent proteasome-mediated degradation. As H1.1 binding dynamics to the nucleosomes are altered, the progressive degradation of H1.1 depletes the available pool for binding. Meanwhile, the lack of translation possibly resulting from a translational quiescence in the SMC, broad or gene specific, prevents the replenishment of the H1.1 pool. As a result, chromatin becomes available to epigenetic modifiers, transcription factors, or both, to render the cell competent for the post-meiotic formation of the gametes.

While the work of Christophorou and colleagues inspired our approach, an initial misalignment in protein sequences led to the serendipitous identification of R57 as a key amino acid for H1.1 eviction. However, R57 is located 12 amino acids upstream of the conserved R54 residue in the mouse H1.2 histone (**Figure S2D**). Future research will investigate whether the *Arabidopsis* R79 residue in H1.1 also contributes its destabilization and degradation in the SMC, and whether H1 destabilization involves a broader mechanism in which several, yet unidentified residues are neutralized. Additionally, phosphorylation is known to be a major destabilizing PTM of H1 at the onset of S-phase, which is crucial for replication in animal cells[57]. The *Arabidopsis* H1.1 variant contains three S/TPxK motifs in the C-tail, that are prone to phosphorylation[56], and CDC2/CDKA;1 can physically interact with H1.1[58]. It remains to be determined whether this mechanism contributes to H1.1 eviction in the SMC prior to meiotic S-phase[19].

The role of citrullination in chromatin regulation has been extensively studied in animal systems, in disease and development. Particularly, histone hypercitrullination is responsible for chromatin decondensation in activated neutrophils upon inflammatory immune response and for the production of chromatin-containing neutrophil extracellular traps [59,60]. PAD enzymes are also associated with oncogenicity where their ectopic activation leads to chromatin decondensation, ectopic histone citrullination and deregulation of gene expression[61,62]. Yet, histone citrullination also plays a role in development. Notably, the citrullination of H1[25] but also of H3 and H4[63] are necessary for activating pluripotency genes in PGCs. After fertilization, selective citrullination of H3 and H4 is necessary for embryonic genome activation and proper gene expression[64].

By contrast, much less is known about citrullination in plants. The catalytic domain of the plant AIH citrulinase is highly conserved with its mammalian PAD4 counterpart: it shares the four key catalytic amino acids and exhibits similar inhibitor sensitivity, indicating that citrullination may play a fundamental role in plants too. Indeed, protein citrullination has recently been identified as a significant post-translational modification in response to cold stress in cell cultures[43]. Our discovery that AIH is required for H1.1 eviction in SMCs opens new avenues for investigating the role of histone citrullination in plant chromatin dynamics.

A key question arising from our findings is the cell specificity of H1.1 degradation. Both AIH and CUL4 are broadly expressed in the ovule primordium, a pattern that does not explain the observed cell-specific degradation. One possibility is that these enzymes might be catalytically regulated by a cofactor conferring cell specificity. For example, mammalian PADI4 activity is influenced by Ca^{2+} availability[65]. In an alternative model, H1.1 destabilization and degradation is the default process in all primordium cells, but, in the SMC, low or stalled transcription and/or translation could prevent replenishment of the H1.1 degraded pool. With an average polyA tail of ~55-60 nt and a half-life of about 1 hour in vegetative tissues, H1.1 transcripts do not exhibit distinctive features [66,67]. However, the short lifetime of H1.1 transcripts in the SMC progenitor, in combination with a relative transcriptional quiescence[19] might be sufficient to prevent the replenishment of H1.1 on chromatin. Whether translational inhibition also occurs in the SMC, targeting specific transcripts such as H1.1, or if it is part of a broader mechanism —similar to what is seen in animal PGCs[68]—remains to be determined. Interestingly, premeiotic spikelets and male meiocytes in prophase I of rice are enriched in phased secondary small interfering RNAs (phasiRNAs) involving MEL1[69] and bearing the potential for translational inhibition[70,71]. Future studies could explore the repertoire of small and antisense

RNAs in the female SMCs of *Arabidopsis*. This model, where H1.1 undergoes rapid turnover throughout the primordium but is not replenished in the SMC due to stalled transcription and/or translation might also apply to other chromatin constituents such as H2A.Z and H3.1/HTR13 variant shown to be specifically lost in the SMC[19,20]. This opens the exciting question of which process(es) specifically reduce transcriptional and/or translational activity in the SMC.

Implications of premeiotic H1.1 clearance for reproduction

H1 eviction from mouse PGCs and subsequent chromatin reorganization are essential for establishing pluripotency in the germline[25]. Although similar events were known to occur during SMC formation in *Arabidopsis*, marking the transition from somatic to reproductive fate[19,23], the precise role of H1 eviction remained unknown. Since linker histones interplay with the deposition and maintenance of various epigenetic marks in *Arabidopsis*, including DNA methylation, histone methylation (including H3K27me3), histone acetylation, and intergenic antisense transcription[72–75], their eviction at the onset of SMC differentiation likely opens a window of opportunity for epigenetic reprogramming. With our current knowledge derived from H1 loss of function mutants, we had expected that SMCs compromised in H1.1 eviction eg $H1.1^{R57K}$ or $H1.1^{K89R}$ would show incomplete chromatin reorganization. In such a scenario, we expected maintenance of heterochromatin instead of the decondensation normally seen in SMC[19], and similar levels of CHH methylation and LHP1-GFP (a H3K27me3 reader) in SMCs and surrounding cells instead of the decrease observed in SMCs [19,21]. We detected mild differences within the $H1.1^{R57K}$-expressing mutant and little to no effect with $H1.1^{K89R/6xGC}$. These distinct outcomes can be explained by a two-step destabilization-degradation model (**Figure 6**). The $H1.1^{R57K}$ mutant, while as stable as the native, uncitrullinated variant, remains more mobile, a characteristic of linker histones. Although the unbound pool forms at a slower rate with $H1.1^{R57K}$, it may still be degraded, albeit more slowly. In contrast, the degradation-resistant $H1.1^{K89R/6xGC}$ mutant remaining citrullinated maintains a pool of H1 that, while less stable, can still bind chromatin and exchange at a higher rate than the wild-type variant.

We found that H1.1 eviction in SMCs is not essential for meiosis but is crucial for establishing the developmental competence of the haploid functional megaspore to produce a functional embryo sac. We propose that premeiotic H1 eviction plays a critical role in establishing an epigenetic landscape in the SMC that primes for the post-meiotic transcriptional program in the functional megaspore, thus controlling its developmental competence. Since the functional

megaspore generates a multicellular embryo sac comprising different cell types, it is pluripotent. Thus, similar to H1 eviction in mouse PGCs, H1 eviction in Arabidopsis SMCs seems necessary to establish pluripotency in the functional megaspore. However, this hypothesis requires further investigation, e.g., through transcriptome analyses of functional megaspores.

Functional megaspores derived from SMCs where H1.1 eviction was disrupted, were compromised in mitosis, resulting in delayed or arrested embryo sac development at the 2-4 cell stage. This finding suggests a failure in the expression of one or several components controlling endomitosis, nuclear migration in the syncytium, cell growth, or a combination thereof. Notably, the H1.1R57K mutant, preventing H1.1 destabilization in SMC chromatin, had a different impact on embryo sac development than the H1.16GC mutant, which abolishes degradation. In the former, embryo sac development was delayed, while in the latter, it was arrested. These findings could be explained by a scenario where although H1.1R57K persists in the SMC, a relevant fraction of H1.1 still undergoes degradation, enabling some degree of epigenomic reprogramming. In contrast, the continuous presence of the H1.16GC mutant, which cannot be degraded, compromises epigenomic reprogramming more severely.

Overall, our study sheds light on the essential role of H1 regulation prior to meiosis to establish post-meiotic competence necessary for embryo sac developmental and thus reproductive success. The parallels observed between plant and animal systems in the regulation of histone dynamics highlight a potential evolutionary convergence in the mechanisms governing reproductive cell fate determination. In both plants and animals, the removal of histone H1 and other chromatin modifications is crucial to establish a chromatin landscape conducive to cell fate transitions [19,22]. Understanding these conserved mechanisms in plants can inform strategies to manipulate reproductive processes in crops, potentially improving fertility and yield.

MATERIAL AND METHODS

Plant growth conditions

Arabidopsis seeds were sterilized in freshly made 0.03% bleach and 0.05% Triton X-100 for 10 min, washed three times in sterile water, briefly incubated in 70% EtOH and washed once before sowing on the germination medium consisting of 0.5xMurashige and Skoog salts (MS, Carolina 19-5700, USA), 10% (w/v) Bactoagar, pH 5.6. Seeds were stratified 2 to 4 days at 4°C before being transferred to a growth incubator (Percival) with long day conditions (16h light [120µE m-2s-1] at 21°C and 8h dark at 16°C). Ten days-post-germination, seedlings at the 2-4 leaves stage were transplanted to soil, covered with a layer of sand and imbibed with Solbac (Andermatt Biocontrol, Switzerland) for pest biocontrol. Plants were grown in a growth chamber with controlled conditions under a long-day photoperiod (16 hours light) at 18-20°C and 38% to 59% rF of humidity.

Generating construct and transgenic lines

The artificial micro-RNAs (amiRNA) targeting CUL4 (At5g46210) or AIH (At5g08170) were designed with the wmd3 database[76] and comprised the following sequences: 5'-ATGC*TCATGATTCGTAGTATA-3' and 5'- ACGC*GAGCCGTTCATTAATTA*-3', respectively, with mismatches to the original sequence indicated by an *. The amiRNAs and the H1.1 mutant variants modified for specific amino acid substitutions were synthesized by Genscript (GenScript Biotech Corporation, genscript.com) and introduced into the *BAR* gene-containing donor vector pRPS5a::LhGR2-GUS::pOP6::attL1-cddb-attL2 vector[31] via Gateway cloning (Thermo Fischer Scientific, USA) according to the manufacturer's recommendation. The resulting constructs, abbreviated as *amiRNA[Cul4]* and *amiRNA[AIH]*, were transformed via *Agrobacterium tumefaciens* (GV3101) into a *pH1.1::H1.1-GFP; pH1.2::H1.2-ECFP*; *3h1 Arabidopsis* line. This line was created by introgressing *pH1.1::H1.1-GFP* and *pH1.2::H1.2-ECFP* into the triple H1 mutant described[19] by crossing and selection. The *pH1.1::H1.1-GFP* line was described [77] and the *pH1.2::H1.2-ECFP* line was created as described for the *pH1.2::H1.2-GFP* line[77] albeit replacing the *GFP* sequence with the *ECFP* sequence (Clontech).

The constructs encoding RFP-tagged H1.1 variants containing codon changes for amino acid substitutions were synthesized by Genscript (GenScript Biotech Corporation, genscript.com), introduced into the same donor vector via Gateway cloning as described above and transformed into the *Arabidopsis* Col-0 accession. Positive T1 plants were identified based on selection for the BAR gene *in vitro* (0.5x MS medium supplemented with 50 µM phosphinothricin) followed

by a GUS reporter assay on the 3rd or 4th true leaf after treatment with 10 µM dexamethasone (see below).

Histochemical detection of GUS reporter activity (GUS reporter assay)

To select transgenic lines with a functional construct we verified each resistant T1 plants for the expression of the *uidA* reporter gene encoding a β-glucuronidase (GUS) and present in the responder cassette[30,31]. For this, one cauline leaf per seedling was incubated with the reaction buffer (0.1% Triton X-100, 10mM EDTA, 2mM ferrocyanide, 2mM ferricyanide, 100mM Na_2HPO_4, 100mM NaH2PO4, 2mg/mL X-Gluc) in 48-multiwell plates, vacuum infiltrated for 5min and stained for 6-8 hours at 37°C.

Dexamethasone treatments

Arabidopsis lines containing the dexamethasone (Dex)-inducible constructs were induced as described[32]. Briefly, flower buds were delicately opened with dissecting needles under the stereomicroscope to allow for a good exposure of the carpel, then gently brushed, using a fine paint brush with soft hairs, either with the induction solution (10 µM Dexamethasone [Sigma-Aldrich Merck KGaA, Germany], 0.1 % DMSO [Sigma-Aldrich Merck KGaA, Germany], 0.01% Silwet-L77, ddH2O) or with a mock solution (0.1 % DMSO, 0.01% Silwet-L77, ddH2O). Flower buds or siliques were collected several days post-induction (dpi) depending on the experiment. The preparation of this material for microscopical analyses is described further below.

Epoxomycin and Cl-amidine treatments

For epoxomycin treatment, intact inflorescences were collected and flower buds older than stage 10[78,79] were removed. The remaining inflorescences were immersed in an epoxomicin-containing solution (5µM epoxomycin (LUCERNA-CHEMÒ), 0.01%Silwet-77L, 0.01%Tween-20, ddH_20) in a 48 multiwell-plate and incubated in a growth incubator (Percival, long days, 21°C) for 2 days before sample preparation for imaging. For Cl-amidine treatment, young flower buds were treated with 1 µM Cl-amidine (CalbiochemÒ) supplemented with 0.01% Silwet-L77 or with a mock solution (0.01 %DMSO, 0.01% Silwet-L77) the same way as for the Dex treatments described above.

Western-blot and quantification

For protein extraction, ~100mg of 10 days old *Arabidopsis* seedlings were harvested and ground using a Retsch homogenizer in liquid nitrogen. The ground tissue was resuspended in

400 µL of SDS lysis buffer (40 mM Tris-HCl pH 7.5, 10% glycerol, 5 mM MgCl2, 4% SDS). The samples were incubated at room temperature for 10 minutes under gentle shaking at 400 rpm (Eppendorf ThermoMixer) to solubilize the tissue evenly in the SDS lysis buffer. Following a centrifugation at 13'000g for 5 min the supernatant was collected, and centrifugated again at 13'000g for 5 min. The final supernatant was collected for protein quantification using the Pierce BCA Protein Assay kit (Thermo Fisher Scientific), following the manufacturer's protocol with 10 µL of the sample/standard. All sample concentrations were normalized by diluting with SDS lysis buffer. The freshly prepared protein samples were then mixed with 1 µL 5x loading buffer (250 mM Tris-HCl pH 6.8, 5% SDS, 50% glycerol, few mg bromophenol blue, 5% β-mercaptoethanol) and boiled for 10 min at 95°C.

For immunoblotting, 10 µg of protein extract was loaded for each sample onto an SDS page gel (Mini-PROTEAN TGX™ Precast Gels, Bio-Rad, #4561094). Electrophoresis was performed at 90V, followed by the transfer of proteins onto a nitrocellulose membrane using the Trans-Blot Turbo Transfer System (Bio-Rad) at 2.5A constant, 25V for 20 min. The membrane was stained 1min with Ponceau red (PanReac AppliChem, Cat#A2935,0500), before acquiring an image with the ChemiDoc Imaging System (Bio-Rad). The membrane was then washed with ddH_2O and blocked with TBS-T (1xTBS, 1% Tween) blocking buffer containing 5% bovine serum albumin (BSA) with shaking for at least 60 min. The membrane was sealed in a plastic pouch and incubated overnight at 4°C on a shaker with 3 mL of primary anti-CUL4 antibody (PhytoAB Cat#PHY0850S) at 1:2000, all diluted in blocking buffer.

Following the primary antibody incubation, the membrane was washed three times for 10 min each with TBS-T before incubation with the secondary HRP-conjugated anti-rabbit IgG antibody (Amersham NA934V Cat#17550629) diluted at 1:10,000 in TBS-T supplemented with 5% milk, for 1h on a shaker. The membrane was washed again three times for 10 min each with TBS-T then incubated for 1 min with 500 µL of Clarity Max Western ECL Substrate (Bio-Rad 1705062) and imaged using the ChemiDoc Imaging System (Bio-Rad). The relative intensity mean was calculated for each sample as the ratio between the intensity mean of the predicted band around CUL4 ~91KDa and the intensity mean of the major band on the Ponceau staining ~70kDa. The ratio was then expressed relative to Line4-Rep2 set to "1". Measurements were done using Fiji on 8bit greyscale inverted images using ROI of the same size.

3D Confocal imaging of whole-mount ovule primordia

Carpels freshly dissected from flower buds were delicately opened using insulin needles to remove the carpel walls and expose the ovule primordia, and mounted in Renaissance solution

(final concentrations: 1:2000 Renaissance;10% glycerol; 0.05% DMSO; 0.1%Triton X-100 in 1x PBS (modified from[33] on a Superfrost™ slide (Thermo Fisher Scientific) and covered with a 18x18mm coverslip, #1.5 thickness (Assistant, Germany) and immediately imaged. Fixed, cleared ovules stained with propidium iodide in acrylamide pads (see below) were mounted in Vectashield (H1300-10, Vector Laboratory, USA) and covered with a 18x18mm coverslip, #1.5 Thickness (Assistant, Germany). Serial image acquisition was carried out using confocal microscopy (CSLM Leica SP5 Resonance, or Stellaris, Leica Microsystems, Germany) with an HC PL APO 63x/1,30 GLYC CORR CS2 objective lens, using the fluorophore's optimal excitation laser, an emission window of circa 40-60nm centered on the emission maximum, using a resonance scanning mode (8000Hz), photon counting mode for detection, and background free HyD detectors, with signal accumulation per line to optimize the pixel intensity distribution. Images were acquired with voxel size of 0.08- 0.1µm x,y,z dimension.

Microscopy-based scoring of the H1 eviction phenotype in female SMCs

The H1.1 eviction phenotype in SMCs was scored on several replicate ovule primordia from independent flower buds under live scanning (see above). Three categories were considered: (i) Full eviction: no detectable signal in the SMC; (ii) Partial eviction: detectable signal, usually in chromocenters; (iii) Persistence: clear signal in both euchromatin and chromocenters. In the main figures, only two categories are shown, persistence and eviction, where the latter comprises both the partial and full eviction categories. In supplemental data, referred to in each relevant figure, the detailed scoring of the three categories is given.

Microscopy-based scoring of ovule stage-specific markers

Ovule primordia expressing the SMC, meiosis and gametophyte specific markers *KNU::nlsYFP*[46], *ASY1::ASY1-YFP*[47] and *AKV::H2B-YFP*[48] respectively, were prepared as described for microscopy analysis. Ovules were scored under live imaging for presence/absence of signal at developmental stages and in genetic backgrounds indicated in the figures and associated data.

For tetrad analysis in ovules, the samples were mounted in Renaissance solution (final concentrations: 1:2000 Renaissance;10% glycerol; 0.05% DMSO; 0.1%Triton X-100 in 1x PBS (modified from[33] . The presence of normal versus abnormal tetrads was scored under live, 3D imaging at stages and in genetic backgrounds indicated in the figures and associated data.

Analysis of embryo sac development

Embryo sac development was analyzed by identifying the developmental stages as described[80], either using the *AKV::H2B-YFP* reporter line[17], introgressed into the mutant backgrounds, or by tissue clearing as indicated in the relevant figures. For tissue clearing, inflorescences were fixed in acetic acid: EtOH solution (3:1) and incubated for at least 4 hours at room temperature. The samples were then transferred in 70% EtOH and mounted in a clearing solution (chloral hydrate: water: glycerol 8:2:1 w/v/w). The samples were analyzed using transmission light microscopy (Leica DMR, Leica Microsystems, Germany) with differential interference contrast (DIC), using a 20x or 40x dry objective (NA 0.75 and 0.5). Images were acquired using a digital camera (Flexacam C3 Leica Microsystems, Germany).

Whole-mount propidium iodide (PI) staining

Whole-mount staining of ovule primordia was done as described[23]. Briefly, Dex-treated flower buds collected at 5dpi were fixed in 1% formaldehyde,10% DMSO in PBS-Tween (0.1%), then dissected and embedded in 5% acrylamide pads on microscope slides. Tissue processing included clarification, cell wall digestion and permeabilization before application of 10µg/ml propidium iodide (PI). Samples were mounted in Vectashield supplemented with PI (Invitrogen)

Image processing for signal quantification, cell volume measurement, and RHF analysis

Image processing for 3D reconstruction, segmentation, signal, or cell size segmentation was performed with the Imaris software (Bitplane, Switzerland). Images presented in the figures correspond to 3D reconstruction or partial z-projections, using orthogonal or oblique slicers, encompassing the SMCs and surrounding cells.

Cell segmentation for cell size measurements was done as described using ImarisCell[81] based on the Renaissance signal in cell walls[33]. Cell volumes of the SMC, the companion cell, and the neighboring cells were exported for analysis.

For quantifying fluorescent reporter signals in nuclei, the later were segmented using Imaris' surface tool, in the semi-automated segmentation mode guided by user-defined manual contours. The sum of voxel intensities (intensity sum) per channel and per nucleus was exported for analysis. If not otherwise indicated, the relative intensity in the SMC was expressed as a ratio between the intensity sum in the SMC nucleus divided by the average intensity sum of 3-4 nuclei from neighboring L2 nucellar cells.

The relative heterochromatin fraction (RHF) was calculated as the sum of intensity sums in the chromocenters (CC) divided by the intensity sum in the nucleus. Measurements were done on

intensity sum projections encompassing the SMC and surrounding nucellus nuclei, processed in Fiji for manual regions-of-interest (ROI) definition.

3D protein structure alignment

The 3D predicted protein structures 1VKP for AIH (green) and 2DEW for PADI4 (yellow) were superimposed in COOT[82] and the result was visualized in PyMOL[83].

Fluorescence Recovery After Photobleaching (FRAP)

Measurements were done on root tips of five days old seedlings essentially as described[84] using a confocal laser scanning microscope equipped with a FRAP module (Leica SP8-R, inverted, Leica microsystems, Germany). Briefly, one sample was prepared at a time, with one root gently mounted (without squashing) in freshly made liquid 0.5x MS. The slide was sealed with transparent nail polish and let to equilibrate for 5-10 min on the microscope stage, with the imaging chamber set at a constant temperature of 20°C. Bleaching and imaging were done using an APO PL 63x water immersion objective, NA 1.4, over a single plane with the pinhole increased up to maximum (5.38 AU) to capture the entire nucleus. Bleaching was performed within a region-of-interest (ROI) of 2µm diameter, positioned in euchromatin, using 3-5 pulses to reach near full bleach of the signal, using the maximal power and full transmission of the 561nm laser. Post-bleach images were recorded using low laser intensity for sustainable acquisition, with two sequences: the first sequence of 30 images with 265ms intervals captures the initial, rapid recovery phase; the second sequence captured the slow recovery phase with 24 images with 10 sec intervals. For analyzing fluorescence recovery, images were first corrected for nuclear drifts occurring during acquisition, using a rigid registration approach in Fiji[85]. Fluorescence measurements were done for the bleached ROI, a background ROI of the same size outside the nucleus, and for the nucleus captured manually with contours. The calculation of fluorescence recovery using double normalization was done as described[86] with intensities at each time point expressed relative to the initial intensity (becoming 1, maximum intensity before bleaching) for each image for comparison.

Fertility analysis

Single inflorescences were induced with either 10µM Dex or a mock solution as previously described. At 19-21 dpi, the 6th, 7th, 8th silique of each treated plant was collected, and the number of infertile ovules (white, shriveled), aborted seeds (brow, shriveled) and viable seeds (green, plump) was scored.

RNA *in situ* hybridization

The antisense RNA probe was designed to target all splicing versions of the *AIH* transcripts (At5g08170) and covers position 441-774 of the coding sequence (see **Figure S3B**). RNA probes were synthesized and labelled using the DIGOXIGENIN (DIG) RNA Labeling Kit (DIG RNA Labeling Mix, Cat.No. 11277073910, Sigma-Aldrich Merck KGaA, Germany) following the manufacturer's instructions. Probe synthesis was performed using the following forward and reverse primers 5'- CGCTTTGGAACGAATTCC-3' and 5'-TAATACGACTCACTATAGGGCCGAAAGAGCTTCCACAG-3', respectively. The *in vitro* transcription reaction was carried out using the T7 RNA polymerase according to the manufacturer's recommendation (Sigma-Aldrich Merck KGaA, Germany). RNA probe preparation and *in situ* hybridizations were done as described [87]. Briefly, single inflorescences (Col_0) were fixed in ice-cold fixative (4% paraformaldehyde (w/v), 1xPBS), embedded in wax using a tissue processor (ASP200, Leica BIOSYSTEMS, Switzerland AG). 6-µm-thick sections were prepared on Superfrost^{TM} Plus Adhesion Microscope Slides (Thermo Fisher Scientific Inc), dewaxed using Histoclear (Sigma-Aldrich Merck KGaA, Germany) and dehydrated using a series of EtOH dilutions. Following Proteinase K digestion, slides were fixed in formaldehyde solution, treated with acetic anhydride and dehydrated using a series of EtOH dilutions. RNA hybridization was performed overnight at 43°C in 50% formamide, 2xSSC. Post-hybridization steps were carried out with a series of formamide dilutions, before washes and dehydration using an EtOH dilution series. Detection was carried out with an anti-digoxigenin antibody conjugated with alkaline phosphatase (AP), 1:700 (Anti-Digoxigenin-AP, Fab fragments, Sigma-Aldrich Merck KGaA, Germany). The chromogenic reaction was performed overnight using the BCIP alkaline phosphatase substrate and NBT catalyst (BCIP/NBT Color Development Substrate, Promega, Switzerland). Slides were analyzed under transmission light microscopy (Leica DMR, Leica Microsystems, Germany) and images were acquired with a digital camera (Flexacam C3, Leica Microsystems, Germany).

Measurement of pollen viability

Flower buds at stages 5-7 were treated with Dex as before and flowers at stage 8– to 9 were collected 9 days post induction (9 dpi). Anthers containing mature pollen were dissected, gently squashed onto slides, and fixed in 10% EtOH for 10 minutes. Samples were then mounted in an Alexander staining solution (10% EtOHEthanol, 0.01% mMalachite green, 25% glycerol, 0.05% acid fuchsin, 0.005% Orange G, 4% glacial acetic acid in distilled water (modified after [88]).

ACKNOWLEDGEMENTS

We thank Diana Pazmino, Valeria Gagliardini, Christoph Eichenberger for technical assistance in plant care, digital qPCR, microscopy, respectively, Sara Simonini and Daniela Guthörl (University of Zurich) for advice with RNA *in situ* hybridization, Stefano Bencivenga (University of Zurich) for advice regarding recalcitrant cloning, Frédérique Pasquer and Ramona Hartman (University of Zurich) for in-house sequencing, Arturo Bolanos and Peter Kopf (University of Zurich) for general lab support, Vimal Rawat (University of Zurich) for help with the expression map of *CULLIN* genes, the central microscopy facility (ZMB) of the University of Zurich for microscopy support, Mathieu Ingouff (IRD Montpellier, France) for the *mCHH-YFP* DynaMet line, Mathew Tucker (University of Adelaide, Australia) for the *KNU::nlsYFP* line, Wei Cai Yang (Institute of Genetics and Developmental Biology, Beijing, China) for the *AKV::H2B-YFP* line, Stefan Heckmann (IPK Gatersleben, Germany) for the *ASY1::ASY1-YFP* line, and Daphné Autran (IRD, Montpellier, France) for critical reading of the manuscript and insightful suggestions.

FUNDING

The project was supported by the University of Zurich, the Swiss National Science Foundation (grants #310030_185186 to CB and #31003A_179553 to UG), and the European Union's Horizon 2020 research and innovation programme under the Marie Sklodowska-Curie (MSC) grant agreement No 847585 (RESPONSE, to CB and SB), and benefitted from networking events of the European Cooperation in Science and Technology (COST) Action # CA16212.

AUTHOR CONTRIBUTIONS

Conceptualization, C.B.; Methodology, Y.L., D.F., J.S., S.B., U.G. and C.B.; Formal Analysis: Y.L., D.F. and C.B.; Investigation, Y.L., D.F., J.S., K.R., A.L., Z.K. and C.B.; Software: A.G.F.; Writing – Original Draft, Y.L. and C.B.; Writing – Review & Editing, Y.L., D.L., U.G. and C.B.; Visualization: Y.L. and C.B.; Funding Acquisition, S.B., U.G. and C.B.; Resources: U.G., S.B. and C.B.; Supervision, SB, UG and C.B.

DECLARATION OF INTERESTS

The authors declare no competing interests.

DECLARATION OF GENERATIVE AI AND AI-ASSISTED TECHNOLOGIES

During the preparation of this manuscript, the authors used ChatGPT OpenAI for text editing purposes (language style and grammar). The authors reviewed and edited the content as needed; they take full responsibility for the content of the publication.

SUPPLEMENTAL INFORMATION

Document S1. Supplemental Figures S1-S6

Document S2. Zipped folder containing six Excel files each containing the Data Source Files 1-6 (raw data for graphs and charts) related to each figure.

REFERENCES

1. Bendel–Stenzel, M., Anderson, R., Heasman, J., and Wylie, C. (1998). The origin and migration of primordial germ cells in the mouse. Seminars in Cell & Developmental Biology *9*, 393–400. https://doi.org/10.1006/scdb.1998.0204.

2. Skinner, D.J., and Sundaresan, V. (2018). Recent advances in understanding female gametophyte development. Preprint at F1000Research, https://doi.org/10.12688/f1000research.14508.1 https://doi.org/10.12688/f1000research.14508.1.

3. Koltunow, A.M., and Grossniklaus, U. (2003). Apomixis: A Developmental Perspective. Annu. Rev. Plant Biol. *54*, 547–574. https://doi.org/10.1146/annurev.arplant.54.110901.160842.

4. Pinto, S.C., Mendes, M.A., Coimbra, S., and Tucker, M.R. (2019). Revisiting the Female Germline and Its Expanding Toolbox. Trends in Plant Science *24*, 455–467. https://doi.org/10.1016/j.tplants.2019.02.003.

5. Lora, J., Yang, X., and Tucker, M.R. (2019). Establishing a framework for female germline initiation in the plant ovule. Journal of Experimental Botany *70*, 2937–2949. https://doi.org/10.1093/jxb/erz212.

6. Jiang, T., and Zheng, B. (2022). Epigenetic Regulation of Megaspore Mother Cell Formation. Front. Plant Sci. *12*, 826871. https://doi.org/10.3389/fpls.2021.826871.

7. Hernandez-Lagana, E., Mosca, G., Mendocilla-Sato, E., Pires, N., Frey, A., Giraldo-Fonseca, A., Michaud, C., Grossniklaus, U., Hamant, O., Godin, C., et al. (2021). Organ geometry channels reproductive cell fate in the *Arabidopsis* ovule primordium. eLife *10*, e66031. https://doi.org/10.7554/eLife.66031.

8. Cai, H., Liu, L., Huang, Y., Zhu, W., Qi, J., Xi, X., Aslam, M., Dresselhaus, T., and Qin, Y. (2022). Brassinosteroid signaling regulates female germline specification in *Arabidopsis*. Current Biology *32*, 1102-1114.e5. https://doi.org/10.1016/j.cub.2022.01.022.

9. Cai, H., Liu, K., Ma, S., Su, H., Yang, J., Sun, L., Liu, Z., and Qin, Y. (2025). Gibberellin and cytokinin signaling antagonistically control female-germline cell specification in *Arabidopsis*. Developmental Cell *60*, 706-722.e7. https://doi.org/10.1016/j.devcel.2024.11.009.

10. Huang, Y., Liu, L., Chai, M., Su, H., Ma, S., Liu, K., Tian, Y., Cao, Z., Xi, X., Zhu, W., et al. (2023). Epigenetic regulation of female germline development through ERECTA signaling pathway. New Phytologist *240*, 1015–1033. https://doi.org/10.1111/nph.19217.

11. Balasubramanian, S., and Schneitz, K. (2000). NOZZLE regulates proximal-distal pattern formation, cell proliferation and early sporogenesis during ovule development in *Arabidopsis* thaliana. Development *127*, 4227–4238. https://doi.org/10.1242/dev.127.19.4227.

12. Wei, B., Zhang, J., Pang, C., Yu, H., Guo, D., Jiang, H., Ding, M., Chen, Z., Tao, Q., Gu, H., et al. (2015). The molecular mechanism of SPOROCYTELESS/NOZZLE in controlling *Arabidopsis* ovule development. Cell Res *25*, 121–134. https://doi.org/10.1038/cr.2014.145.

13. Lieber, D., Lora, J., Schrempp, S., Lenhard, M., and Laux, T. (2011). *Arabidopsis* WIH1 and WIH2 Genes Act in the Transition from Somatic to Reproductive Cell Fate. Current Biology *21*, 1009–1017. https://doi.org/10.1016/j.cub.2011.05.015.

14. Grossniklaus, U., and Schneitz, K. (1998). The molecular and genetic basis of ovule and megagametophyte development. Semin Cell Dev Biol *9*, 227–238. https://doi.org/10.1006/scdb.1997.0214.

15. Zhao, X., Bramsiepe, J., Van Durme, M., Komaki, S., Prusicki, M.A., Maruyama, D., Forner, J., Medzihradszky, A., Wijnker, E., Harashima, H., et al. (2017). RETINOBLASTOMA RELATED1 mediates germline entry in *Arabidopsis*. Science *356*, eaaf6532. https://doi.org/10.1126/science.aaf6532.

16. Cao, L., Wang, S., Venglat, P., Zhao, L., Cheng, Y., Ye, S., Qin, Y., Datla, R., Zhou, Y., and Wang, H. (2018). *Arabidopsis* ICK/KRP cyclin-dependent kinase inhibitors function to ensure the formation of one megaspore mother cell and one functional megaspore per ovule. PLOS Genetics *14*, e1007230. https://doi.org/10.1371/journal.pgen.1007230.

17. Schmidt, A., Wuest, S.E., Vijverberg, K., Baroux, C., Kleen, D., and Grossniklaus, U. (2011). Transcriptome Analysis of the *Arabidopsis* Megaspore Mother Cell Uncovers the Importance of RNA Helicases for Plant Germline Development. PLoS Biol *9*, e1001155. https://doi.org/10.1371/journal.pbio.1001155.

18. Hou, Z., Liu, Y., Zhang, M., Zhao, L., Jin, X., Liu, L., Su, Z., Cai, H., and Qin, Y. (2021). High-throughput single-cell transcriptomics reveals the female germline differentiation trajectory in *Arabidopsis* thaliana. Commun Biol *4*, 1–16. https://doi.org/10.1038/s42003-021-02676-z.

19. She, W., Grimanelli, D., Rutowicz, K., Whitehead, M.W.J., Puzio, M., Kotliński, M., Jerzmanowski, A., and Baroux, C. (2013). Chromatin reprogramming during the somatic-to-reproductive cell fate transition in plants. Development *140*, 4008–4019. https://doi.org/10.1242/dev.095034.

20. Hernandez-Lagana, E., and Autran, D. (2020). H3.1 Eviction Marks Female Germline Precursors in *Arabidopsis*. Plants *9*, 1322. https://doi.org/10.3390/plants9101322.

21. Ingouff, M., Selles, B., Michaud, C., Vu, T., Berger, F., Schorn, A., Autran, D., Van Durme, M., Nowack, M., Martienssen, R., et al. (2017). Live-cell analysis of DNA methylation during sexual reproduction in *Arabidopsis* reveals context and sex-specific dynamics controlled by noncanonical RdDM. Genes & Development *31*. https://doi.org/10.1101/gad.289397.116.

22. Hajkova, P., Ancelin, K., Waldmann, T., Lacoste, N., Lange, U.C., Cesari, F., Lee, C., Almouzni, G., Schneider, R., and Surani, M.A. (2008). Chromatin dynamics during epigenetic reprogramming in the mouse germ line. Nature *452*, 877–881. https://doi.org/10.1038/nature06714.

23. She, W., and Baroux, C. (2014). Chromatin dynamics during plant sexual reproduction. Front. Plant Sci. *5*. https://doi.org/10.3389/fpls.2014.00354.

24. Izzo, A., Ziegler-Birling, C., Hill, P.W.S., Brondani, L., Hajkova, P., Torres-Padilla, M.-E., and Schneider, R. (2017). Dynamic changes in H1 subtype composition during epigenetic reprogramming. Journal of Cell Biology *216*, 3017–3028. https://doi.org/10.1083/jcb.201611012.

25. Christophorou, M.A., Castelo-Branco, G., Halley-Stott, R.P., Oliveira, C.S., Loos, R., Radzisheuskaya, A., Mowen, K.A., Bertone, P., Silva, J.C.R., Zernicka-Goetz, M., et al. (2014). Citrullination regulates pluripotency and histone H1 binding to chromatin. Nature *507*, 104–108. https://doi.org/10.1038/nature12942.

26. Zhang, Y., Cooke, M., Panjwani, S., Cao, K., Krauth, B., Ho, P.-Y., Medrzycki, M., Berhe, D.T., Pan, C., McDevitt, T.C., et al. (2012). Histone H1 Depletion Impairs Embryonic Stem Cell Differentiation. PLoS Genet *8*, e1002691. https://doi.org/10.1371/journal.pgen.1002691.

27. Vierstra, R.D. (1993). Protein Degradation in Plants. Annual Review of Plant Biology *44*, 385–410. https://doi.org/10.1146/annurev.pp.44.060193.002125.

28. Yang, Q., Zhao, J., Chen, D., and Wang, Y. (2021). E3 ubiquitin ligases: styles, structures and functions. Mol Biomed *2*, 23. https://doi.org/10.1186/s43556-021-00043-2.

29. Chen, H., Shen, Y., Tang, X., Yu, L., Wang, J., Guo, L., Zhang, Y., Zhang, H., Feng, S., Strickland, E., et al. (2006). *Arabidopsis* CULLIN4 Forms an E3 Ubiquitin Ligase with RBX1 and the CDD Complex in Mediating Light Control of Development. Plant Cell *18*, 1991–2004. https://doi.org/10.1105/tpc.106.043224.

30. Craft, J., Samalova, M., Baroux, C., Townley, H., Martinez, A., Jepson, I., Tsiantis, M., and Moore, I. (2005). New pOp/LhG4 vectors for stringent glucocorticoid-dependent transgene expression in *Arabidopsis*: Inducible expression from improved pOp promoters. The Plant Journal *41*, 899–918. https://doi.org/10.1111/j.1365-313X.2005.02342.x.

31. Samalova, M., Kirchhelle, C., and Moore, I. (2019). Universal Methods for Transgene Induction Using the Dexamethasone-Inducible Transcription Activation System pOp6/LhGR in *Arabidopsis* and Other Plant Species. Current Protocols in Plant Biology *4*, e20089. https://doi.org/10.1002/cppb.20089.

32. Schubert, J., Li, Y., Mendes, M.A., Fei, D., Dickinson, H., Moore, I., and Baroux, C. (2022). A procedure for Dex-induced gene transactivation in *Arabidopsis* ovules. Plant Methods *18*, 41. https://doi.org/10.1186/s13007-022-00879-x.

33. Musielak, T.J., Schenkel, L., Kolb, M., Henschen, A., and Bayer, M. (2015). A simple and versatile cell wall staining protocol to study plant reproduction. Plant Reprod *28*, 161–169. https://doi.org/10.1007/s00497-015-0267-1.

34. Jerzmanowski, A. (2004). The linker histones. In New Comprehensive Biochemistry Chromatin Structure and Dynamics: State-of-the-Art. (Elsevier), pp. 75–102. https://doi.org/10.1016/S0167-7306(03)39004-0.

35. Chen, Z., Chen, Y.-Z., Wang, X.-F., Wang, C., Yan, R.-X., and Zhang, Z. (2011). Prediction of Ubiquitination Sites by Using the Composition of k-Spaced Amino Acid Pairs. PLoS ONE *6*, e22930. https://doi.org/10.1371/journal.pone.0022930.

36. Radivojac, P., Vacic, V., Haynes, C., Cocklin, R.R., Mohan, A., Heyen, J.W., Goebl, M.G., and Iakoucheva, L.M. (2010). Identification, analysis, and prediction of protein ubiquitination sites. Proteins *78*, 365–380. https://doi.org/10.1002/prot.22555.

37. Walton, A., Stes, E., Cybulski, N., Van Bel, M., Iñigo, S., Durand, A.N., Timmerman, E., Heyman, J., Pauwels, L., De Veylder, L., et al. (2016). It's Time for Some "Site"-Seeing: Novel Tools to Monitor the Ubiquitin Landscape in *Arabidopsis thaliana*. Plant Cell *28*, 6–16. https://doi.org/10.1105/tpc.15.00878.

38. Wiśniewski, J.R., Zougman, A., Krüger, S., and Mann, M. (2007). Mass Spectrometric Mapping of Linker Histone H1 Variants Reveals Multiple Acetylations, Methylations, and Phosphorylation as Well as Differences between Cell Culture and Tissue. Molecular & Cellular Proteomics *6*, 72–87. https://doi.org/10.1074/mcp.M600255-MCP200.

39. Brown, D.T., Izard, T., and Misteli, T. (2006). Mapping the interaction surface of linker histone H10 with the nucleosome of native chromatin in vivo. Nat Struct Mol Biol *13*, 250–255. https://doi.org/10.1038/nsmb1050.

40. Dumbliauskas, E., Lechner, E., Jaciubek, M., Berr, A., Pazhouhandeh, M., Alioua, M., Cognat, V., Brukhin, V., Koncz, C., Grossniklaus, U., et al. (2011). The *Arabidopsis* CUL4–DDB1 complex interacts with MSI1 and is required to maintain MEDEA parental imprinting. The EMBO Journal *30*, 731–743. https://doi.org/10.1038/emboj.2010.359.

41. Martinsen, J.H., Saar, D., Fernandes, C.B., Schuler, B., Bugge, K., and Kragelund, B.B. (2022). Structure, dynamics, and stability of the globular domain of human linker histone H1.0 and the role of positive charges. Protein Science *31*, 918–932. https://doi.org/10.1002/pro.4281.

42. Klepikova, A.V., Kasianov, A.S., Gerasimov, E.S., Logacheva, M.D., and Penin, A.A. (2016). A high resolution map of the *Arabidopsis thaliana* developmental transcriptome based on RNA -seq profiling. The Plant Journal *88*, 1058–1070. https://doi.org/10.1111/tpj.13312.

43. Marondedze, C., Elia, G., Thomas, L., Wong, A., and Gehring, C. (2021). Citrullination of Proteins as a Specific Response Mechanism in Plants. Front. Plant Sci. *12*, 638392. https://doi.org/10.3389/fpls.2021.638392.

44. Luo, Y., Arita, K., Bhatia, M., Knuckley, B., Lee, Y.-H., Stallcup, M.R., Sato, M., and Thompson, P.R. (2006). Inhibitors and Inactivators of Protein Arginine Deiminase 4: Functional and Structural Characterization ·. Biochemistry *45*, 11727–11736. https://doi.org/10.1021/bi061180d.

45. Exner, V., Aichinger, E., Shu, H., Wildhaber, T., Alfarano, P., Caflisch, A., Gruissem, W., Köhler, C., and Hennig, L. (2009). The Chromodomain of LIKE HETEROCHROMATIN PROTEIN 1 Is Essential for H3K27me3 Binding and Function during *Arabidopsis* Development. PLoS ONE *4*, e5335. https://doi.org/10.1371/journal.pone.0005335.

46. Tucker, M.R., Araujo, A.-C.G., Paech, N.A., Hecht, V., Schmidt, E.D.L., Rossell, J.-B., De Vries, S.C., and Koltunow, A.M.G. (2003). Sexual and Apomictic Reproduction in *Hieracium* subgenus *Pilosella* Are Closely Interrelated Developmental Pathways. Plant Cell *15*, 1524–1537. https://doi.org/10.1105/tpc.011742.

47. Valuchova, S., Mikulkova, P., Pecinkova, J., Klimova, J., Krumnikl, M., Bainar, P., Heckmann, S., Tomancak, P., and Riha, K. (2020). Imaging plant germline differentiation within *Arabidopsis* flowers by light sheet microscopy. eLife *9*, e52546. https://doi.org/10.7554/eLife.52546.

48. Rotman, N., Durbarry, A., Wardle, A., Yang, W.C., Chaboud, A., Faure, J.-E., Berger, F., and Twell, D. (2005). A Novel Class of MYB Factors Controls Sperm-Cell Formation in Plants. Current Biology *15*, 244–248. https://doi.org/10.1016/j.cub.2005.01.013.

49. She, W., and Baroux, C. (2015). Chromatin dynamics in pollen mother cells underpin a common scenario at the somatic-to-reproductive fate transition of both the male and female lineages in *Arabidopsis*. Front. Plant Sci. *6*. https://doi.org/10.3389/fpls.2015.00294.

50. Moon, J., Parry, G., and Estelle, M. (2004). The Ubiquitin-Proteasome Pathway and Plant Development. The Plant Cell *16*, 3181–3195. https://doi.org/10.1105/tpc.104.161220.

51. Mazzucotelli, E., Belloni, S., Marone, D., Leonardis, A.M.D., Guerra, D., Fonzo, N.D., Cattivelli, L., and Mastrangelo, A.M. (2006). The E3 Ubiquitin Ligase Gene Family in Plants: Regulation by Degradation. Current Genomics *7*, 509–522. https://doi.org/10.2174/138920206779315728.

52. Biedermann, S., and Hellmann, H. (2011). WD40 and CUL4-based E3 ligases: lubricating all aspects of life. Trends in Plant Science *16*, 38–46. https://doi.org/10.1016/j.tplants.2010.09.007.

53. Fonseca, S., and Rubio, V. (2019). *Arabidopsis* CRL4 Complexes: Surveying Chromatin States and Gene Expression. Front. Plant Sci. *10*. https://doi.org/10.3389/fpls.2019.01095.

54. Lian, J.-P., Yang, Y.-W., He, R.-R., Yang, L., Zhou, Y.-F., Lei, M.-Q., Zhang, Z., Huang, J.-H., Cheng, Y., Liu, Y.-W., et al. (2021). Ubiquitin-dependent Argonauteprotein MEL1 degradation is essential for rice sporogenesis and phasiRNA target regulation. The Plant Cell *33*, 2685–2700. https://doi.org/10.1093/plcell/koab138.

55. Xue, H., Zhang, Q., Wang, P., Cao, B., Jia, C., Cheng, B., Shi, Y., Guo, W.-F., Wang, Z., Liu, Z.-X., et al. (2022). qPTMplants: an integrative database of quantitative post-translational modifications in plants. Nucleic Acids Research *50*, D1491–D1499. https://doi.org/10.1093/nar/gkab945.

56. Kotliński, M., Rutowicz, K., Kniżewski, Ł., Palusiński, A., Olędzki, J., Fogtman, A., Rubel, T., Koblowska, M., Dadlez, M., Ginalski, K., et al. (2016). Histone H1 Variants in *Arabidopsis* Are Subject to Numerous Post-Translational Modifications, Both Conserved and Previously Unknown in Histones, Suggesting Complex Functions of H1 in Plants. PLoS ONE *11*, e0147908. https://doi.org/10.1371/journal.pone.0147908.

57. Alexandrow, M.G., and Hamlin, J.L. (2005). Chromatin decondensation in S-phase involves recruitment of Cdk2 by Cdc45 and histone H1 phosphorylation. J Cell Biol *168*, 875–886. https://doi.org/10.1083/jcb.200409055.

58. Pusch, S. (2012). Identification of kinase substrates by bimolecular complementation assays. The Plant Journal *70*, 348–356. https://doi.org/10.1111/j.1365-313X.2011.04862.x.

59. Maronek, M., and Gardlik, R. (2022). The Citrullination-Neutrophil Extracellular Trap Axis in Chronic Diseases. Journal of Innate Immunity *14*, 393–417. https://doi.org/10.1159/000522331.

60. Zhu, Y.P., Speir, M., Tan, Z., Lee, J.C., Nowell, C.J., Chen, A.A., Amatullah, H., Salinger, A.J., Huang, C.J., Wu, G., et al. (2023). NET formation is a default epigenetic program controlled by PAD4 in apoptotic neutrophils. Science Advances *9*, eadj1397. https://doi.org/10.1126/sciadv.adj1397.

61. Zhu, D., Zhang, Y., and Wang, S. (2021). Histone citrullination: a new target for tumors. Molecular Cancer *20*, 90. https://doi.org/10.1186/s12943-021-01373-z.

62. Zheng, Q., Osunsade, A., and David, Y. (2020). Protein arginine deiminase 4 antagonizes methylglyoxal-induced histone glycation. Nat Commun *11*, 3241. https://doi.org/10.1038/s41467-020-17066-y.

63. Xiao, S., Lu, J., Sridhar, B., Cao, X., Yu, P., Zhao, T., Chen, C.-C., McDee, D., Sloofman, L., Wang, Y., et al. (2017). SMARCAD1 Contributes to the Regulation of Naive Pluripotency by Interacting with Histone Citrullination. Cell Rep *18*, 3117–3128. https://doi.org/10.1016/j.celrep.2017.02.070.

64. Zhang, X., Liu, X., Zhang, M., Li, T., Muth, A., Thompson, P.R., Coonrod, S.A., and Zhang, X. (2016). Peptidylarginine deiminase 1-catalyzed histone citrullination is essential for early embryo development. Sci Rep *6*, 38727. https://doi.org/10.1038/srep38727.

65. Arita, K., Hashimoto, H., Shimizu, T., Nakashima, K., Yamada, M., and Sato, M. (2004). Structural basis for Ca2+-induced activation of human PAD4. Nat Struct Mol Biol *11*, 777–783. https://doi.org/10.1038/nsmb799.

66. Jia, J., Lu, W., Liu, B., Fang, H., Yu, Y., Mo, W., Zhang, H., Jin, X., Shu, Y., Long, Y., et al. (2022). An atlas of plant full-length RNA reveals tissue-specific and monocots–dicots conserved regulation of poly(A) tail length. Nat. Plants *8*, 1118–1126. https://doi.org/10.1038/s41477-022-01224-9.

67. Szabo, E.X., Reichert, P., Lehniger, M.-K., Ohmer, M., de Francisco Amorim, M., Gowik, U., Schmitz-Linneweber, C., and Laubinger, S. (2020). Metabolic Labeling of RNAs Uncovers Hidden Features and Dynamics of the *Arabidopsis* Transcriptome[CC-BY]. The Plant Cell *32*, 871–887. https://doi.org/10.1105/tpc.19.00214.

68. Oulhen, N., Swartz, S.Z., Laird, J., Mascaro, A., and Wessel, G.M. (2017). Transient translational quiescence in primordial germ cells. Development *144*, 1201–1210. https://doi.org/10.1242/dev.144170.

69. Komiya, R., Ohyanagi, H., Niihama, M., Watanabe, T., Nakano, M., Kurata, N., and Nonomura, K.-I. (2014). Rice germline-specific Argonaute MEL1 protein binds to phasiRNAs generated from more than 700 lincRNAs. The Plant Journal *78*, 385–397. https://doi.org/10.1111/tpj.12483.

70. Jiang, P., Lian, B., Liu, C., Fu, Z., Shen, Y., Cheng, Z., and Qi, Y. (2020). 21-nt phasiRNAs direct target mRNA cleavage in rice male germ cells. Nat Commun *11*, 5191. https://doi.org/10.1038/s41467-020-19034-y.

71. Liu, Y., Teng, C., Xia, R., and Meyers, B.C. (2020). PhasiRNAs in Plants: Their Biogenesis, Genic Sources, and Roles in Stress Responses, Development, and Reproduction. The Plant Cell *32*, 3059–3080. https://doi.org/10.1105/tpc.20.00335.

72. Wierzbicki, A.T., and Jerzmanowski, A. (2005). Suppression of histone H1 genes in *Arabidopsis* results in heritable developmental defects and stochastic changes in DNA methylation. Genetics *169*, 997–1008. https://doi.org/10.1534/genetics.104.031997.

73. Rutowicz, K., Lirski, M., Mermaz, B., Teano, G., Schubert, J., Mestiri, I., Kroteń, M.A., Fabrice, T.N., Fritz, S., Grob, S., et al. (2019). Linker histones are fine-scale chromatin architects modulating developmental decisions in *Arabidopsis*. Genome Biology *20*, 157. https://doi.org/10.1186/s13059-019-1767-3.

74. Zemach, A., Kim, M.Y., Hsieh, P.-H., Coleman-Derr, D., Eshed-Williams, L., Thao, K., Harmer, S.L., and Zilberman, D. (2013). The *Arabidopsis* nucleosome remodeler DDM1 allows DNA methyltransferases to access H1-containing heterochromatin. Cell *153*, 193–205. https://doi.org/10.1016/j.cell.2013.02.033.

75. Choi, J., Lyons, D.B., Kim, M.Y., Moore, J.D., and Zilberman, D. (2020). DNA Methylation and Histone H1 Jointly Repress Transposable Elements and Aberrant Intragenic Transcripts. Molecular Cell *77*, 310-323.e7. https://doi.org/10.1016/j.molcel.2019.10.011.

76. Meyers, B.C., and Green, P.J. eds. (2010). Plant MicroRNAs: Methods and Protocols (Humana Press) https://doi.org/10.1007/978-1-60327-005-2.

77. Rutowicz, K., Puzio, M., Halibart-Puzio, J., Lirski, M., Kotliński, M., Kroteń, M.A., Knizewski, L., Lange, B., Muszewska, A., Śniegowska-Świerk, K., et al. (2015). A Specialized Histone H1 Variant Is Required for Adaptive Responses to Complex Abiotic Stress and Related DNA Methylation in *Arabidopsis*. Plant Physiol *169*, 2080–2101. https://doi.org/10.1104/pp.15.00493.

78. Smyth, D.R., Bowman, J.L., and Meyerowitz, E.M. (1990). Early flower development in *Arabidopsis*. Plant Cell *2*, 755–767. https://doi.org/10.1105/tpc.2.8.755.

79. Yu, S.-X., Zhou, L.-W., Hu, L.-Q., Jiang, Y.-T., Zhang, Y.-J., Feng, S.-L., Jiao, Y., Xu, L., and Lin, W.-H. (2020). Asynchrony of ovule primordia initiation in *Arabidopsis*. Development, dev.196618. https://doi.org/10.1242/dev.196618.

80. Schneitz, K., Hulskamp, M., and Pruitt, R.E. (1995). Wild-type ovule development in *Arabidopsis* thaliana: a light microscope study of cleared whole-mount tissue. Plant J *7*, 731–749. https://doi.org/10.1046/j.1365-313X.1995.07050731.x.

81. Mendocilla Sato, E., and Baroux, C. (2017). Analysis of 3D Cellular Organization of Fixed Plant Tissues Using a User-guided Platform for Image Segmentation. BIO-PROTOCOL *7*. https://doi.org/10.21769/BioProtoc.2355.

82. Emsley, P., Lohkamp, B., Scott, W.G., and Cowtan, K. (2010). Features and development of Coot. Acta Crystallogr D Biol Crystallogr *66*, 486–501. https://doi.org/10.1107/S0907444910007493.

83. Chaudhari, R., and Li, Z. (2015). PyMine: a PyMOL plugin to integrate and visualize data for drug discovery. BMC Res Notes *8*, 517. https://doi.org/10.1186/s13104-015-1483-3.

84. Rosa, S. (2018). Measuring Dynamics of Histone Proteins by Photobleaching in *Arabidopsis* Roots. Methods Mol Biol *1675*, 455–465. https://doi.org/10.1007/978-1-4939-7318-7_26.

85. Schindelin, J., Arganda-Carreras, I., Frise, E., Kaynig, V., Longair, M., Pietzsch, T., Preibisch, S., Rueden, C., Saalfeld, S., Schmid, B., et al. (2012). Fiji: an open-source platform for biological-image analysis. Nat Methods *9*, 676–682. https://doi.org/10.1038/nmeth.2019.

86. Rosa, S., Ntoukakis, V., Ohmido, N., Pendle, A., Abranches, R., and Shaw, P. (2015). Cell Differentiation and Development in *Arabidopsis* Are Associated with Changes in Histone Dynamics at the Single-Cell Level. The Plant Cell *26*, 4821–4833. https://doi.org/10.1105/tpc.114.133793.

87. Dreni, L., Jacchia, S., Fornara, F., Fornari, M., Ouwerkerk, P.B.F., An, G., Colombo, L., and Kater, M.M. (2007). The D-lineage MADS-box gene OsMADS13 controls ovule identity in rice. The Plant Journal *52*, 690–699. https://doi.org/10.1111/j.1365-313X.2007.03272.x.

88. Peterson, R., Slovin, J.P., and Chen, C. (2010). A Simplified Method for Differential Staining of Aborted and Non-Aborted Pollen Grains. International Journal of Plant Biology *1*, e13. https://doi.org/10.4081/pb.2010.e13.